

VOLCANIC MORPHOLOGY OF THE EAST PACIFIC RISE CREST 9° 49' - 52' N:  
IMPLICATIONS FOR EXTRUSION AT FAST-SPREADING MID-OCEAN RIDGES

A THESIS SUBMITTED TO THE GRADUATE DIVISION OF  
THE UNIVERSITY OF HAWAII IN PARTIAL FULFILLMENT  
OF THE REQUIREMENTS FOR THE DEGREE OF  
MASTER OF SCIENCE  
IN  
GEOLOGY AND GEOPHYSICS  
AUGUST 1998

By

Gregory J. Kurras



Thesis Committee:

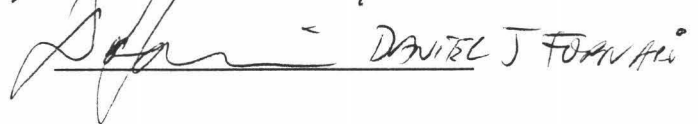
Margo Edwards, Chairperson  
Dan Fornari  
John Sinton  
Charlie Morgan

We certify that we have read this thesis and that, in our opinion, it is Satisfactory in scope and quality as a thesis for the degree of Master of Science in Geology and Geophysics.

THESIS COMMITTEE

  
Chairperson

  
DANIEL J. FORNARI

## ABSTRACT

In an effort to further our understanding of the recent volcanic history of the East Pacific Rise (EPR) in the area of the 1991 volcanic eruption [Haymon et al., 1993; Rubin et al., 1994] we examine the structure and morphology of the axial summit and eastern flank along the EPR crest between  $9^{\circ} 49' - 52'N$ . The distribution of lava morphologies along and across the axis provides some first-order constraints on the dynamics of submarine basaltic lava emplacement with respect to the structure of the ridge crest, and the nature of eruptive activity along this portion of the EPR crest over the past  $\sim 30$  ka. Variations in structure of the ridge and distributions of the lava morphologies support the hypothesis of off-axis volcanism either through off-axis transport or off-axis eruptions, and suggest that this ridge crest has experienced at least three distinctly different types of volcanic emplacement processes. (1) Axial summit eruptions within the near-axis ( $< 0.5$  km off-axis) region are the dominant constructional volcanic mechanism for the extrusion and emplacement of lava. (2) Off-axis transport of lavas erupted at or near the Axial Summit Collapse Trough (ASCT) [Fornari et al., 1997], either through lava tubes or surface flows [e.g. Haymon et al., 1993; Fornari et al., 1998], occurs to at least  $\sim 1.5$  km off-axis and contributes to the accumulation of the extrusive oceanic layer. (3) Off-axis eruptions and local constructional volcanism may account for the formation of a broad crestal plateau east of the ASCT. These processes interact at different spatial and temporal scales along the crest of this 4-th order fast-spreading ridge segment to form the upper oceanic crust at the ridge axis and upper crestal flank ( $\sim 1.5$  km). The region surveyed corresponds to the region over which crustal seismic layer 2A, believed to correspond to the extrusive oceanic layer, attains full thickness [Christeson et al., 1994, 1996; Hooft et al., 1996;

Carbotte et al., 1997]. The regional percentages, a first order approximation of the number of flow units along the ridge crest, and the inferred relative ages of the lava morphologies suggest the contribution of off-axis volcanism to the accumulation of the upper oceanic extrusive layer is significant.

## TABLE OF CONTENTS

|   |     |
|---|-----|
| Abstract .....  | iii |
| Preface .....   | vi  |
| Chapter 1: The Axial Summit .....                       | 1   |
| Abstract .....  | 1   |
| Introduction .....                                      | 1   |
| Data Acquisition, Processing, and Analysis .....        | 3   |
| <i>Navigation</i> .....                                 | 3   |
| <i>Altimetry and Bathymetry</i> .....                   | 4   |
| <i>Data Quality Analysis</i> .....                      | 6   |
| Discussion .....  | 7   |
| Conclusion .....  | 9   |
| Acknowledgements .....                                  | 9   |
| Chapter 2: The Axial Flank .....                        | 11  |
| Abstract .....  | 11  |
| Introduction .....                                      | 12  |
| <i>Previous Geologic Mapping at the MOR Crest</i> ..... | 14  |
| Data Acquisition and Analysis .....                     | 17  |
| Discussion .....  | 25  |
| Conclusions .....                                       | 28  |
| Acknowledgements .....                                  | 31  |
| Appendix A: Tables .....                                | 32  |
| Appendix B: Figures .....                               | 35  |
| References .....  | 48  |

## PREFACE

This thesis examines volcanism along the axial summit and the near-axis Eastern flank of the East Pacific Rise (EPR) 9° 49' - 51'N. The goal of the thesis is to study the eruption dynamics and emplacement processes that have been occurring along this segment of the EPR over the past ~30 ka to better understand the formation of the upper extrusive layer of oceanic crust. The first half of the thesis investigates the structure and morphology of the axial summit using high-resolution bathymetry and near-bottom imagery, and has been published in *Geophysical Research Letters* April 15, 1998. The second half of the thesis investigates the structure and morphology of the eastern ridge flank out to ~1.5 km using Seabeam bathymetry data and near-bottom imagery, and has been submitted for publication to *Marine Geophysical Research* May 1998. Greg Kurras has been the lead author and main contributor, with guidance and input from Dr. Margo Edwards and Dr. Dan Fornari, for both publications.

# CHAPTER 1

## THE AXIAL SUMMIT

### **Abstract**

Bathymetric data acquired during six cruises to the East Pacific Rise crest 9° 49'-51'N are compiled into a single bathymetric database and used to create high-resolution bathymetry maps of two geologically and biologically active areas. Scanning sonar and Alvin altimetry were collected during 23 Alvin dives to the P-vent/Bio9 and Biomarker-141 areas during 1991-95. Bathymetry data were filtered, edited, and processed as individual dives then combined into a single database for each cruise and statistically evaluated. Cruise data sets were numerically and visually compared and cross-correlated to known bottom features and fixed seafloor reference markers, then horizontally shifted to establish a consistent database with 3 m vertical and 5 m horizontal resolutions. The compiled and corrected bathymetry was used to produce bathymetric maps of two areas within the axial summit collapse trough; a  $2 \times 10^4 \text{ m}^2$  area around P and Bio9 vents, and a  $1.1 \times 10^3 \text{ m}^2$  area around Biomarker 141. The resulting detailed bathymetry maps reveal topography dominated by low-relief volcanic constructional features and post-eruptive collapse of lobate and sheet lava surfaces.

### **Introduction**

The axis and flanks of the East Pacific Rise (EPR) between the Siqueiros and Clipperton transforms have been the subject of intense geological and geophysical study for nearly a decade at scales ranging from 0.1 - 100 kms using multibeam sonar and

multichannel seismic data to scales  $<1$  m using near-bottom observations and sonar data collected using the submersible Alvin. The spatial and temporal scales over which tectonic and magmatic processes interact at this fast-spreading ( $110 \text{ mmy}^{-1}$ ) mid-ocean ridge (MOR) are reflected in the range of volcanic, hydrothermal, and structural features observed on the ridge crest and flanks, and how they have evolved over time. Increasing the spatial resolution with which one can map morphological features at the MOR axis during periodic field programs to the same site provides an ability to conduct detailed multidisciplinary investigations of MOR processes over time scales equivalent to the frequency of surveys (months to decades). This approach was used with multibeam data from the Juan de Fuca Ridge to identify areas which had experienced submarine eruptions [Fox et al., 1992; Chadwick et al., 1995]. These investigators demonstrated the viability of establishing and comparing multiple bathymetric data sets to detect topographic changes for a given region over time periods of 1 to  $\sim 10$  yrs.

The type of volcanic constructional topography created at the intermediate-spreading rate Juan de Fuca Ridge is largely pillow lavas [Embley et al., 1994]. This lava morphology creates features that are  $>10\text{-}20$  m high and  $>\sim 1 \times 10^4 \text{ m}^2$  in area, which are easily detected and monitored by repeat multibeam surveys. At fast-spreading MORs, lobate lava flows are generally  $\ll 10$  m thick and topographic variability of constructional volcanic terrain at the axis is subtle. Mapping seafloor structure and monitoring topographic changes with repeat surveys on fast spreading MORs thus requires mapping techniques that can resolve features  $\ll 10$  m high and  $1 \times 10^2 \text{ m}^2$  in area.



This paper discusses the compilation, processing, and analysis bathymetry acquired using the submersible Alvin for two well-studied areas of the EPR crest within the axial summit collapse trough (ASCT) [Fornari et al., in press], in a region which experienced a submarine eruption in 1991 [Haymon et al., 1993; Gregg et al., 1996a]. This work has resulted in very detailed bathymetry for two areas: (1) P and Bio9 vents near  $9^{\circ} 50.3'N$ , and (2) Biomarker 141 near  $9^{\circ} 49.9'N$  (Figure 1).

## **Data Acquisition, Processing, & Analysis**

### *Navigation*

Data used in our analysis were recorded on 19 Alvin dives in the P and Bio9 vent area over the period 1991-95, and 11 dives at the Biomarker 141 site during 1993-95 (Table 1). The key components of our analysis involve editing of individual dive tracks, statistical analysis of combined cruise data sets, cross-correlation of Alvin navigation for each cruise to known bottom features and reference markers, and lateral correction of each cruise data set.

Alvin navigation is calculated using acoustic travel-times from long-baseline, bottom-moored transponders every 15 s. Transponders were surveyed using iterative triangulation of acoustic travel times from the surface ship, whose position was determined using P-code GPS at horizontal distances approximately equal to the water depth. Final position of each transponder was based on ~80-200 fixes resulting in a geographic position error of 1-3 m rms. Haymon et al. [1991] and Fornari et al. [in press] estimate overall Alvin position accuracy and repeatability at 5-10 m. Transponder locations during the various dive programs in the study area are shown in Figure 1.

Three transponders deployed during the Adventure II cruise (denoted by black squares in Figure 1) served as permanent transponders from Jan. 1992 until Dec. 1995, providing consistent navigational references from cruise to cruise. They were serviced in 1996 and redeployed.

Post-processing of Alvin navigation began with outlier removal to eliminate any Alvin positions with horizontal jumps  $>60$  m between consecutive 15 s fixes (this equates to a speed of 3.9 knots, roughly four times Alvin's maximum speed of  $\sim 1$  knot). Navigation time series (latitude vs. time, longitude vs. time, depth vs. time) and spatial series (latitude vs. longitude) were plotted and edited to remove positions with location shifts due to transponder dropouts. Edited position data were run through a 2 min. median filter to reduce noise then sub-sampled into 2 s records. Alvin's raw and processed dive tracks were plotted, compared, and checked against dive log records, previous dive tracks, and known bottom marker locations. Dive tracks were combined into a single latitude, longitude, depth file for each cruise then co-registered against bathymetric features and Biomarkers in the two detailed survey areas. Final lateral shifts for each cruise were determined using a combination of numerical and visual comparison between mapped features and known bottom reference points and are shown in Table 2.

### *Altimetry and Bathymetry*

Bathymetry data were separated into two data types (Alvin bathymetry and Mesotech bathymetry) produced by four instruments mounted on Alvin (675kHz Mesotech Model-1971 scanning altimeter, 100kHz Benthos-2110 altimeter, 200kHz Datasonics-PSA 900-3 altimeter, and Paroscientific-410K-101 pressure transducer).

Variation in sensor position is estimated at ~1 m vertical, ~1-2 m horizontal. The vertical and slope resolution of each instrument is estimated at  $\ll 1$  m. These errors are included within the estimated navigational positioning errors. Combining Alvin's pressure depth and its distance above the bottom produced Alvin bathymetry. The pressure transducer has a resolution of 1.0 PSIA (~2 m) and both altimeters have resolution  $\ll 1$  m resulting in bathymetry data with a statistically combined resolution of 3 m. (Note: In May 1994 a change was made in Alvin's algorithm used to convert pressure to depth in meters. This necessitated the adjustment of the altimetry data collected before that date to maintain a consistent vertical reference frame relative to later cruises.) Mesotech data are a series of acoustic ranges to the seafloor relative to the mount location on Alvin and accurate to  $\ll 1$  m resolution. Mesotech ranges were combined with pressure depth, the smoothed interpolated 2 sec position and attitude data from Alvin, then converted into geographically independent depth values using software provided by D. Scheirer [pers. comm., 1997].

The depth range in this area is 2490-2540 m as determined from Seabeam data collected in 1994 (Figure 1). Data were automatically filtered to remove information collected from altitudes outside the 1-99 m range, jumps between consecutive pings exceeding 60 m, bathymetry outliers outside the 2490-2540 m range, and then examined and edited on an individual dive basis to remove more subtle errors. Resulting filtered and geographically registered Mesotech and Alvin bathymetry data were combined into a single bathymetric file for each dive with a statistically combined vertical resolution of 3 m.

### *Data Quality Analysis*

The compiled, processed Mesotech and Alvin bathymetry data were combined into a single database for each of the six cruises. Data were binned into 1 m<sup>2</sup> grid cells for each separate study area. Data quality was checked with statistical analysis of the standard deviation, number of data points, magnitude of variation, maximum, minimum, median, and mean of each 1 m<sup>2</sup> bin (Figure 2). Figure 2 shows that the data range is significantly higher than the standard deviation. This is typical of the data sets in that a single or few data points with >4m magnitude variations are enough to effect the range without significantly effecting the standard deviation due to relatively low variations and high data density as seen in the “data density plot”. Areas with high standard deviation (>1.5) and large data range magnitudes (>4 m) were examined on a dive by dive basis to determine which dive for that cruise was introducing the error. The overall quality of the data is demonstrated by the Nov. 1995 data shown in Figure 2. For all cruises, our statistical analyses show consistently low standard deviations with high data density and low depth ranges suggesting that there is excellent internal agreement of these data within each cruise. Position quality was checked by cruise to cruise comparison and cross referencing of bottom features. Final bathymetric grids were made for each detailed survey area at a 0.25 m<sup>2</sup> grid spacing, a 1.5 m<sup>2</sup> data resolution, with an estimated error resolution of 5 m horizontal and 3 m vertical (Figure 3). The contouring algorithm combined the processed and corrected bathymetric data from each cruise, and ran the data through an interative increasing mean filter window function with 0.25 m<sup>2</sup> step increments starting at 0.25 m<sup>2</sup> and finishing at 1.5 m<sup>2</sup>. Each interation step combined the original 0.25 m<sup>2</sup> data with the mean filter output for input into the next larger filter

window size, thereby preserving the original data while averaging progressively larger areas. This process effectively grows the data from the raw data points allowing interpolation at double the maximum filter window size (in this case 3 m<sup>2</sup>). The main advantages over standard surfacing techniques are the elimination of artificial regions created by interpolation over areas with little or no data, and the lack of the “ringing effect” common to surfacing algorithms [A.M. Goodliffe & F. Martinez, per. comm., 1997]. Data presented in these grids represent the mean value of the combined bathymetric data sets from each dive program that have been processed, analyzed, and co-registered to Biomarkers, and seafloor hydrothermal or volcanic features observed from Alvin or recorded in the video data.

## **Discussion**

Figure 3 shows the compiled processed bathymetric data for two areas within the axial summit collapse trough; a  $2 \times 10^4$  m<sup>2</sup> area around P and Bio9 vents, and a  $1.1 \times 10^3$  m<sup>2</sup> area around Biomarker 141. Several key features are observed in the bathymetric maps of the ASCT in the two areas (Figure 3). In comparing the two areas, it is apparent that the mean depth of the trough floor is ~6-8 m shallower in the Biomarker 141 area, while the rim of the ASCT and tops of lava pillars [Gregg and Chadwick, 1996] in both areas are at depths of ~2500-2502 m. The topographic gradient within the floor of the ASCT over the length of the BioTransect [Fornari, et al, in press; Shank et al., in press] shallows towards the south and may reflect local ponding of the 1991 flow over this region. Fornari and Embley [1995] combined Seabeam bathymetry with 1991-93 Alvin altimetry at a 20 m grid-interval. Their bathymetry shows several small, elongate ~5 m

topographic highs displaced just east of the ASCT which are thought to have resulted from flooding and subsequent lava breakout from the trough during the 1991 eruption, and local volcanic construction along the ASCT rim. Visual observations from Alvin confirm that the ASCT was breached in many places by the 1991 flow, and that tops of many lava pillars throughout the study areas generally conform to the depth level of the adjacent ASCT rim [Gregg et al., 1996b].

The P-vent / Bio9 area map (Figure 3) shows an irregular summit trough 8-10 m deep that trends NNW-SSE, parallel to the general trend of the EPR axis. Each area in Figure 3 is characterized by very irregular topography on a scale of 2-6 m with many features represented by closed-contour highs or lows representing near vertical relief. These dimensions are consistent with constructional volcanic features, lava pillars, and collapsed portions of sheet and lobate lava flows in these areas documented by Alvin observations and video recordings [Haymon et al., 1991,1993; Fornari et al., in press; Shank et al., in press]. The ~100 m section of the eastern ASCT wall near the P vent /Bio9 area shows many salients and reentrants at scales of ~5-10 m. Broad irregularities in the plan-view outline of the trough margin at a scale of 50-100 m (Figure 3) are similar to subaerial lava tubes and channel terrain in Hawaii. The deepest portions of the trough floor in the P-vent / Bio9 area occur along a NNW-SSE trending linear zone which delimits the area of eruptive fissuring produced by the 1991 eruption. The somewhat larger, deeper area of collapsed lobate and sheet lava surfaces surrounding P-vent (Figure 3) conforms to a collapse pit surrounding this vent; a site of intense hydrothermal activity just following the eruption in April 1991 [Haymon et al., 1993]. Features apparent in the bathymetry east of the Biomarker 141 location (Figure 3) correlate to visual observations

of the morphology this area which consists of a discontinuous section of the eruptive fissure, flanked to the west by a low (2 m relief) pressure ridge in the corrugated-sheet lava surface [Shank et al., in press].

## **Conclusion**

We have produced high-resolution bathymetric maps by correcting, co-registering, and digitally compiling bathymetric data collected on 23 Alvin dives from a ~4 km long segment of the EPR between 9° 49'-51'N over the period 1991-95. Processing and statistical evaluation of vehicle pressure depth and altitude from 100 kHz and 675 kHz sensors, combined with numerical and visual comparison to bottom features and fixed reference markers can produce compiled bathymetric data with 3 m vertical and 5 m horizontal resolution. The accuracy of two maps produced for the P-vent / Bio9 and Marker 141 areas are of sufficient resolution to resolve volcanic morphology that can be used to characterize the spatial scales over which tectonic and magmatic forces interact at this fast spreading ridge. These data provide a baseline high-resolution bathymetric data set with resolution sufficient to measure future topographic changes caused by eruptions of thin lobate or sheet lava flows, as well as changes in locations and distribution of prominent hydrothermal vents.

## **Acknowledgments**

We thank our coPIs and the crews on the various Adventure dive programs: R. Haymon, M. Lilley, R. Lutz, M. Perfit, T. Shank, P. Shanks, and K. Von Damm for their cooperation in collecting the Mesotech data. L. Abrams of the Alvin group provided

important technical information regarding sensors and data collection methods on Alvin. D. Scheirer and W. Chadwick provided computer code used to process the Mesotech data. P. Wessel and S. Zisk provided assistance with code used to edit, process, and analyze navigation and bathymetric data. This work was supported by National Science Foundation Grant: NSF-OCE-9100503 (DJF and MHE). SOEST Contribution No. 4591, HIGP Contribution No. 982, WHOI Contribution No. 9647.



## CHAPTER 2

### THE AXIAL FLANK

#### **Abstract**

In an effort to further our understanding of the recent volcanic history of the East Pacific Rise (EPR) crest in the area of the 1991 volcanic eruption [Haymon et al., 1993; Rubin et al., 1994] we collected five photographic transects along the EPR crest between 9° 49' - 52' N (Figure 4). The distribution of lava morphologies along and across the axis provides some first-order constraints on the dynamics of submarine basaltic lava emplacement with respect to the structure of the ridge crest, and the nature of eruptive activity along this portion of the EPR crest over the past ~30 ka. Variations in structure of the ridge and distributions of the lava morphologies support the hypothesis of off-axis volcanism either through off-axis transport or off-axis eruptions, and suggest that this ridge crest has experienced at least three distinctly different types of volcanic emplacement processes. (1) Axial summit eruptions within the near-axis (< 0.5 km off-axis) region are the dominant constructional volcanic mechanism for the extrusion and emplacement of lava. (2) Off-axis transport of lavas erupted at or near the Axial Summit Collapse Trough (ASCT) [Fornari et al., 1997], either through lava tubes or surface flows [e.g. Haymon et al., 1993; Fornari et al., 1998], occurs to at least ~1.5 km off-axis and contributes to the accumulation of the extrusive oceanic layer. (3) Off-axis eruptions and local constructional volcanism may account for the formation of a broad crestal plateau east of the ASCT. These processes interact at different spatial and temporal scales along the crest of this 4-th order fast-spreading ridge segment to form the upper oceanic crust at

the ridge axis and upper crestal flank (~1.5 km). The region surveyed corresponds to the region over which crustal seismic layer 2A, believed to correspond to the extrusive oceanic layer, attains full thickness [Christeson et al., 1994, 1996; Hooft et al., 1996; Carbotte et al., 1997]. The regional percentages, a first order approximation of the number of flow units along the ridge crest, and the inferred relative ages of the lava morphologies suggest the contribution of off-axis volcanism to the accumulation of the upper oceanic extrusive layer is significant.

## **Introduction**

The global mid-ocean ridge (MOR) crest is one of the most active volcanic system on the Earth, yet only a very small portion of it has been studied in detail to understand its volcanic and magmatic history. Despite the abundance of volcanic activity at the MOR crest, only a few eruptions have been documented on intermediate and fast-spreading ridges in the past five years. Technical limitations and logistical difficulties make it hard to remotely monitor MOR volcanic events and access the sea floor during or just after eruptions [Haymon et al., 1993; Dziak et al., 1995; Embley et al., 1995, 1996; Fox and Dziak, 1996, in press; Fox et al., 1997; Gregg et al., submitted]. In Hawai'i or Iceland, lava flow dynamics and eruptive history are well-studied through various observational and remote-sensing techniques, however, the constraints imposed by the global nature and deep ocean environment of the MOR crest make it challenging to study the dynamics of submarine lava flow emplacement.

It is the combination of detailed and repeated observations, geologic sampling, and geophysical remote sensing data that allows us to map the distribution of lava flows and

deduce the fine-scale volcanic stratigraphy. This information, combined with analyses of the lavas to determine their petrological and geochemical characteristics, helps us to better understand the internal structure of a volcano. During the past ~15 years marine geological, geophysical, and petrological data have provided valuable insights into the morphological, structural, and magmatic processes that control volcanism at the fast-spreading East Pacific Rise (EPR) [e.g. Macdonald et al., 1984; Lonsdale, 1985; Thompson et al., 1985; Langmuir, 1986; Macdonald and Fox, 1988; Sinton and Detrick, 1992; Harding et al., 1993; Perfit et al., 1994; Fornari et al., 1998]. Regional studies of the MOR crest have been augmented by relatively few detailed investigations using either submersibles or towed cameras to map the volcanic terrain and sample the lavas [e.g. Ballard and Van Andel, 1977; Lonsdale, 1977; Ballard et al., 1981; 1982, 1984; Gente et al., 1986; Haymon et al., 1991, 1993; Chadwick and Embley, 1994; Fornari et al., 1998]. In order to understand the dynamics of submarine lava emplacement one has to relate observations of submarine volcanic morphology and the distribution of volcanic facies to the regional and local topography of the ridge crest and its magmatic processes. Recent, empirical and theoretical modeling of submarine lava emplacement, and comparison of submarine to subaerial basaltic lava emplacement processes have been extremely useful in guiding our understanding of how lava erupts at the MOR crest and how the rheology of the lava affects its morphology [e.g. Bonatti et al., 1988; Griffiths et al., 1992; Gregg and Fink, 1995; Gregg et al., 1996].

In an effort to further our understanding of the recent volcanic history of the EPR crest in the area of the 1991 volcanic eruption [Haymon et al., 1993; Rubin et al., 1994] we collected five photographic transects along the EPR crest between 9° 49' - 52'N

(Figure 4). This portion of the ridge has been spreading at  $55 \text{ mm yr}^{-1}$  (half-rate) for at least the past  $\sim 1 \text{ ma}$  [Carbotte and Macdonald, 1992]. The line spacing shown in Figure 4 was chosen to provide along-axis traverses of volcanic terrain on the east flank of the crestal plateau created at  $\sim 5 \text{ ka}$  to  $10 \text{ ka}$  intervals over the region where the crustal seismic layer 2A attains its full thickness [e.g. Christeson et al., 1994, 1996; Hooft et al., 1996; Carbotte et al., 1997]. Our conceptual approach in carrying out these camera surveys was that by studying the distribution of lava morphologies along and across the axis we could provide some first-order constraints on the dynamics of submarine basaltic lava emplacement with respect to the structure of the ridge crest, and better understand the eruptive activity along this portion of the EPR crest over the past  $\sim 30 \text{ ka}$ .

### ***Previous Geologic Mapping at the MOR Crest***

In order to provide some perspective on the methods we used, and the impact of these types of studies to our understanding of MOR volcanism, we have focused on two of the earliest, most comprehensive efforts to produce geologic maps of the MOR crest: the FAMOUS project along the slow-spreading Mid-Atlantic Ridge (MAR)  $36^{\circ} 30'$  to  $37^{\circ} \text{ N}$  [Ballard and Van Andel, 1977], and the Galapagos Rift survey [Ballard et al., 1982] near  $86^{\circ} \text{ W}$ . The FAMOUS project [Ballard and Van Andel, 1977] used *Alvin* to make direct observations of seafloor lava morphology and geologic features along the inner rift valley of the MAR. These observations, combined with bathymetric and geophysical data, were used to create a geologic map of the area which showed an asymmetric distribution of morphologies along the inner rift valley floor. This investigation revealed a complex interaction of volcanic and tectonic processes that we know now vary both temporally

and spatially at various scales along the entire global MOR system [Macdonald et al., 1984; Lonsdale, 1985; Francheteau and Ballard, 1983; Macdonald and Fox, 1988; Carbotte et al., 1997; Embley et al., 1995; Fornari et al., 1998; Haymon et al., 1991; 1993; Haymon, 1996; Perfit and Chadwick, 1998].

The Galapagos Rift survey near 86°W [Ballard et al., 1982] used photographs from the ANGUS towed camera system, multibeam bathymetry and observations from *Alvin* to create detailed maps of volcanic features and their relationships to active hydrothermal systems. Using this information to map the lava flows, the distributions of lava morphology, and the ages of lava flows, they demonstrated an along-axis volcanic variability along the Galapagos Rift that suggested a complex temporal and spatial variation in MOR magmatic supply. A model that included volcanic cycles punctuated by increased effusion, or fluctuation in eruptive volume related to spreading rate and magmatic supply was suggested to account for this along-axis volcanic and morphologic variation seen at the Galapagos Rift at 86W [Laughton and Searle, 1979; Ballard et al., 1982].

More recently, several investigators have studied the relationship between magmatic and tectonic processes at the MOR crest and how those integrated processes lead to the construction of the oceanic crustal layer. Better seismic imaging of the crust and upper mantle using multichannel (MCS) geophysical techniques, and near-bottom geophysical experiments have greatly improved our understanding of MOR crustal structure, its variability, and the presence of zones where magma or partially molten rock may be present. Despite these improvements, seismic imaging only provides a snapshot in time of the subsurface structure, and an effective averaging of the physical properties and

characteristics of the various layers. Seismic data alone, can not produce detailed volcanic stratigraphy and bare-rock drilling into the upper oceanic crust at a fast spreading MOR has, to date, proven to be very difficult [Storms and Batiza, 1992]. Sinton and Detrick [1992] used seismic and petrological/geochemical data to develop conceptual relationships between MCS data, MOR volcanism, axial morphology, and the variability of magmatic supply along a ridge crest. Other investigators have focused on understanding the relationships between hydrothermal processes at the ridge axis, magmatic supply, and ridge spreading rate [e.g. Macdonald and Fox, 1988; Haymon et al., 1991, 1993; Humphris, 1995; Fornari and Embley, 1995; Haymon, 1996]. Christeson et al. [1992, 1994, 1996], Hooft et al. [1996], and Carbotte et al. [1997] examined the detailed structure and spatial characteristics of seismic layer 2A and have tried to understand the development of this important upper crustal layer within a context of the temporal and spatial variability of volcanism and magmatism along the MOR. The new seismic model of layer 2A indicates that the accumulation of extrusive volcanics increases to its constant thickness usually within ~2 km of the spreading axis [Christeson et al., 1992; 1994; 1996; Hooft et al., 1996; Carbotte et al., 1997].

Many current accretionary models for the EPR are focusing on the hydrothermal and volcanic processes occurring within the narrow (~ <1 km wide) axial zone [e.g. Haymon et al., 1991, 1993; Haymon, 1996; Fornari et al., 1998]; however, off-axis volcanism is also suspected to be important. A growing body of geological and petrological evidence indicates that off-axis eruptions occur [e.g. Perfit et al., 1994; Goldstein et al., 1997, Sims et al., 1997], implying that these eruptions may contribute significant volumes of material to the formation of the extrusive oceanic layer [e.g. Perfit et al., 1994; Gregg et al., 1996;

Macdonald et al., 1996; Sims et al., 1997; Perfit and Chadwick, 1998]. To examine the contribution of off-axis volcanism to the accumulation of the extrusive layer, we must examine the fine scale stratigraphy and morphology of the upper oceanic crust over the region in which the crustal seismic layer 2A, believed to correspond to the extrusive oceanic layer, attains its full thickness [Christeson et al., 1994, 1996; Hooft et al., 1996; Carbotte et al., 1997]. Using a towed camera system to collect photographic transects over this extrusive accumulation zone, we studied the distribution of lava morphologies and volcanic features to interpret the eruptive history and emplacement processes acting along this fast-spreading EPR crest 9° 49' - 51' N over the past ~30 ka.

### **Data Acquisition and Analysis**

The WHOI towed camera is a self-contained digital and 35mm camera system towed from a surface ship using a standard 0.680 inch steel dredge wire [Fornari and Spencer, 1998; Fornari et al., 1998]. Ridge parallel survey lines were run at 0.5 km and 0.25 km west of the ASCT, within the ASCT, and to the east of the ASCT by 0.5 km, 0.75 km, 1.0 km, and 1.5 km (Figure 4). Digital images and 35mm pictures were acquired every 15 sec at altitudes of ~5 to 10 m above the seafloor as determined by a 12 kHz pinger trace. Typical tow speeds averaged ~0.25 knots (~8 m/min) which produced a spacing of ~1 - 2 m between pictures and with 80 - 100% along track coverage (Figure 5). Navigation of the towed camera was done using a layback calculation and P-Code GPS positions of the surface ship every 15 sec. The tow camera data were supplemented by visual observations and down-looking video collected during *Alvin* dives 2770, 2771, and 2772, which traversed the EPR crest and upper flanks in 1994 [Cochran et al., 1996; submitted]

(Figure 4). Navigation of the *Alvin* dives was by bottom-moored transponders which has been shown to be accurate to ~5 - 8 m [Haymon et al., 1991; Fornari et al., 1998; Kurras et al., 1998].

Imagery from each camera tow and *Alvin* dive was analyzed and compiled into a database that contains all the volcanic and morphologic identifiers, and relevant topographic and structural information. Examples of these data are shown in Figure 6 and summarized in Table 3. The occurrence of apparent flow contacts, variations in sediment cover and sediment infilling between the volcanic forms, and other geologic observations were noted and are cross-referenced based on image location. Images were classified into five main categories of lava morphology and four transitional categories shown in Figure 7 and listed in Table 3. The forms and nomenclature of the lava morphology classifications used in this paper are consistent with those used in Ballard and Van Andel [1977] and Ballard et al., [1982; 1984]. The three categories of sheet lava (lineated, ropy, and hackly lava) were combined into a single sheet lava category for the purpose of our overall analysis and discussion.

Figures 8 and 9 summarize the distributions and percentages of the lava morphologies we have mapped. With the exception of the inset shown in Figure 8, the percentages are relative and have not been normalized to the length of each survey line; consequently they do not reflect regional morphologic distributions. However, the variations in distribution and relative percentages are useful in assessing the style of volcanism that this segment of the EPR has experienced for the past ~ 30ka.

Lobate lava comprises the largest percentage (66%) of the three morphology classifications (Figure 8). They are extensively distributed both along and across-axis



within the surveyed area (Figure 9). *Alvin* dives in the area also identified numerous flow contacts in the lobate lava, based on the glassiness of the lava and contact relationships, which suggest the existence of multiple lobate flow units throughout the axial summit region between 9° 49' N - 52' N.

Pillow lava is the least abundant morphology, comprising only 10% of the surveyed area. Pillows are more abundant at distances >0.5 km from the ASCT, especially in the northern half of the survey area (Figure 9). Comparison of pillow lava distribution data in Figure 9 with the local ridge crest morphology shown in the topographic profiles in Figure 10, suggests that the areas where pillow lava have been emplaced often coincide with a topographic bench in the crestal flank east of the ASCT (Figure 10, #1 and #2 symbols).

Sheet lava comprises 18% of the morphologic distribution over the surveyed area (Figure 8). Though mainly concentrated around the axial summit high (Figures 8 and 9), sheet lava occurs throughout the region, and tends to occur in small focused clusters. Variations in surface texture of the three types of sheet lava (lineated, ropy, hackly) (Figure 6) can be used to infer emplacement properties at the time of deposition; however, for the purpose of our numerical and statistical analysis, the three different sheet lava morphologies were classified into a single "sheet lava" category as shown in Figures 8 and 9. Although we do not use the three different sheet flow morphologies in the numerical analysis, the distinctions were used when examining the data for flow contacts.

Table 4 summarizes our analysis of flow contacts as determined from the photo-transects along the ridge crest. Flows were differentiated based on changes in sediment

cover on or sediment infill between the lava forms, changes in the lava morphology that are not flow transitions (i.e. change in surface morphology of the same eruptive unit), changes in the lava glassiness, and distinct flow-contact relationships. The upper bound for each type of change indicates the maximum number of inferred flow contacts recorded for that survey line segment (Table 4). The lower bound is the number of unique descriptions (ie. 30%, 40%, 50% sediment cover) for that particular type of change. These values vary for each individual survey line segment, and reflect minimum number of flow contacts found along that line based on changes in surface character (ie. sediment, morphology, glassiness). The nature and volume of the imagery data from our photographic transects make it very difficult to unequivocally distinguish flow contacts without creating a continuous photo-mosaic of the entire survey line, imagery that would probably take up the entire floor of a high-school gymnasium. The impracticality of such a mosaic means we were forced to use some subjective judgement and make an approximation of the number of flow contacts that exist along each survey line segment. On the basis of that rationale and considering the number of lava flows that one might count along the southern slope of the East Rift Zone of Kilauea, we have chosen the average number of flow contacts. Normalizing this value to the length of each survey line segment, we estimate the number of flow contacts per kilometer along-axis (Table 4). Near axis (<0.5 km) we find ~7 flow contacts per kilometer and off-axis (>0.5 km) only ~5 flow contacts per kilometer. This information suggests that there are more flow contacts along-axis within the near axis (~0.5 km) zone than exists within the crestal region at distances >0.5 km from the ASCT. Though the count of flow contacts is only a first-order approximation, the relative distribution of these flow contacts is useful and

provides insight into the eruptive history of the ridge crest. Past efforts have tried to quantify the average number of eruptions over a given time period based upon volcanological, geochemical, and morphological constraints (Chadwick and Embley, 1998; Fornari et al., 1998; Haymon et al., 1996; Rubin et al., 1994). Using an approximation of one eruption along a 10 - 50 km length of the EPR every 5 - 8 years, with nearly constant spreading over the past ~30 ka, one arrives at an estimate of 3,750 - 6,000 eruptions. Normalizing the minimum number of eruptions to the maximum unit length of ridge, we estimate 75 eruptions per kilometer of ridge axis. In light of these estimates, based on numbers suggested by other researchers, and considering the repeated volcanic overprinting that occurs in any volcanic system, our approximations of flow contacts and the average number of flow contacts per kilometer of ridge (Table 4) seem more reasonable.

Figure 10 shows the cross-sectional variation of the EPR crest between 9° 49' and 52'N using bathymetric profiles calculated from the 1994 Seabeam bathymetry data every 100 m along-axis. The local-scale variation in the ridge crest structure can be correlated, on a regional scale, to the distribution of volcanic morphologies mapped using the towed camera data. The northern area (Figure 10A) has the smallest cross-sectional area and displays a consistent and prominent bench near the middle (Figure 10A #1) of each of the profiles. This bench (Figure 10A #1) roughly correlates with the greater abundance of pillow lavas in this area. The roll-off at the eastern end of these northern profiles is also more abrupt than for the southern two areas. The central set of profiles (Figure 10B) shows the greatest variability along strike, especially near the eastern margin of the ASCT. The slope of the eastern flank of the crest is fairly consistent (~1.2°), shallower

than that displayed by the northern and southern set of profiles; it also displays greater variability. The minimum slope and maximum cross-sectional area [Scheirer and Macdonald, 1993] are both located within this middle region near the axial summit high ( $\sim 9^{\circ} 50.3' N$ ), although the cross-sectional area for this one mile segment of the ridge is only marginally greater than that of the southern segment shown in Figure 10C. The southern set of profiles (Figure 10C) is also tightly clustered indicating a consistent and steeper slope to the east of the ASCT. To the extreme east of the ASCT there is a small bench (Figure 10C #2) that correlates with a second concentration of pillow lavas. The southern and northern profiles display the most variability in seafloor slope and topography just to the west of the ASCT, whereas the central profiles show a very consistent seafloor slope west of the ASCT.

Figure 11 shows lava morphology as a function of regional topographic slope, as calculated from the 1994 Seabeam data, to demonstrate that all of the volcanic morphologies we mapped occur over the entire range of calculated slopes. Ninety-nine percent of the data fall within slope angles which range from  $0^{\circ}$  to  $4^{\circ}$ ; only 1% of the data lie in the range of  $4^{\circ}$  to  $8^{\circ}$ . These slope values are based on 50 m gridded Seabeam data, not near-bottom profiles, which could account for the homogenization of the slope values to all the volcanic morphologies. However, using slopes derived from near-bottom profiles collected during *Alvin* dives, we find that this distribution of morphology over the range of topographic slope is nearly the same as it is for slope calculated from the multibeam data; slope values range from  $0^{\circ}$  -  $8^{\circ}$  for 80% of the *Alvin* data. Though only an approximation, this type of slope measurement is still useful as a first order

approximation of ridge crest gradients and shows the range and distributions of volcanic morphologies and correlation with slope.

The photo-mosaic of a small off-axis lineated sheet flow (Figure 5) ~0.5 km west of the ASCT and flowing down slope (westward) shows the interaction of flow morphology and local scale topographic slope. The top of the mosaic shows a transition of the sheet flow from a lineated to a hackly sheet, formed as the flow lost velocity and spilled out of the contained channel. These types of very localized transitions demonstrate the important effects that effusion rate and local pre-flow topography have in controlling submarine lava flow morphology.

The photo-transects presented in Figures 12 and 13 show images of lobate and sheet lava across the ridge axis (see Figure 9 for the locations of the photo-transects). These photos illustrate the variation in the glassiness of the lava, sediment infill between the lava forms, sediment cover on the lava, surface texture of the lava, and morphologic flow contacts. Similar to the analysis of the data for flow contacts (Table 4), changes in these lava characteristics and the presence of geologic features such as fissures and faults can be used to infer relative ages of the lava. The lobate lava of Figure 12 (LOB-1 and LOB-2) and Figure 13 (LOB-3) show an increase in sediment cover and sediment infill between the lava forms, as well as an increase in surface roughness and decrease in lava glassiness. These trends in lava characteristics lead us to conclude that, in general, the age of the lava increases with increasing distance off-axis. However, Figure 13 (SH-1) does not show an increase in apparent lava age with increasing distance off-axis. Photo-transect SH-1 demonstrates the similar surface texture and apparent lack of sediment cover on a hackly sheet flow located in photographs taken 0.60 km, 0.75 km, and 1.5 km

east of the ASCT. Although this sheet lava was emplaced upon crust with presumed magnetic age differences that span ~10 ka to 15 ka, it is difficult to distinguish an age difference between the photographs of hackly lava shown in transect SH-1 which covers a lateral distance of ~1000 m. The hackly sheet lava of photo-transect SH-1 (G) and the lobate lava of LOB-3 (D) are both ~1.5 km east of the ASCT and are located ~300 m apart (Figure 9). Though not conclusive, the character and inferred age of the hackly sheet suggest it may be ~30 ka younger than the crust upon which it is emplaced, and that it could have erupted at or near the ASCT and flowed at least ~1.5 km down the eastern flank of the EPR crest.

The relationships between lava morphology and terrain we have presented have implications for extrusive volcanic processes occurring along the EPR crest 9° 49' - 52' N. Lava morphology can be directly related to the effects of lava viscosity, pre-existing terrain, and lava effusion rate. Investigations into the emplacement mechanisms and processes of subaerial and submarine basaltic eruptions [e.g. Shaw, 1969; Walker, 1973; Hulme, 1974; Moore, 1975; Malin, 1980; Peterson et al., 1980; Bonatti et al., 1988] help constrain our conceptual understanding of eruptive conditions that produce submarine volcanic morphologies. Recent work on the dependency of morphology upon slope angle, flow volume, and effusion rate [e.g. Rowland and Walker, 1990; Griffiths et al., 1992; Hon et al., 1994; Gregg and Fink, 1995; Gregg et al., 1996; 1998] demonstrate some of the key physical properties and relationships that affect basaltic eruptions on the seafloor. This research provides a theoretical framework of key physical properties that allow us to relate observed lava morphologies and the results of our lava morphology

analysis for this small segment of a fast-spreading MOR to the temporal and spatial variations in volcanic processes along the EPR crest over the past ~30ka.

## **Discussion**

The morphology of the lava is determined at the time of emplacement by a complex interaction among pre-existing terrain, lava viscosity, and effusion rate [Bonatti et al., 1988; Gregg and Fink, 1995]. Using photographs from a towed camera system to document the morphology along the EPR crest 9° 49' - 52' N, we infer the eruptive conditions and volcanic history of this fast-spreading MOR over the past ~30 ka. Petrological and geochemical data from samples, rock cores and Alvin samples, collected from the EPR ~9° 30' N [Perfit et al., 1994; 1995; 1996; Smith et al., 1997] indicate that the viscosity and eruption temperature of lavas across and along this region of the ridge crest do not vary greatly. Consequently, we predict that pre-eruption topography and effusion rate are the dominant factors controlling the lava morphology at this fast-spreading MOR.

The structure of the ridge axis, the distributions and relative percentages of the lava morphologies suggest that this ridge crest has experienced at least three distinctly different types of volcanic emplacement processes. (1) Axial summit eruptions within the near axis (< 0.5 km) region are the dominant constructional volcanic mechanism for the extrusion and emplacement of lava. (2) Off-axis transport of lavas erupted at or near the ASCT, either through lava tubes or surface flows [e.g. Haymon et al., 1993; Fornari et al., 1998], occur to at least ~1.5 km off-axis and contribute to the accumulation of the extrusive oceanic layer. (3) Off-axis eruptions and local constructional volcanism may

account for the formation of a broad crestral plateau east of the ASCT. These processes have interacted at different spatial and temporal scales along the crest of this 4th order MOR segment to form the upper oceanic crust at the ridge axis and upper crestral flank.

The regional ridge crest structure shown by the bathymetric data (Figures 4 and 10) and our analysis of morphology and slope (Figure 11) suggest that lobate lavas occur over the entire range of topographic slopes seen within this area. Therefore, we infer that lava morphology along the crest of the EPR in this region is mainly a function of effusion rate. Using the percentages and distributions of lobate lava shown in Figures 8 and 9, both along and across-axis, to infer effusion rate for the ridge axis over the past ~30 ka, we suggest that this ridge segment has been experiencing fairly uniform eruptive activity along the ridge crest 9° 49' - 52' N over this time period.

The axial summit high shown by the bathymetry depicted in Figures 4 and 10 is widely acknowledged as the area of greatest volcanic and magmatic activity along this 4th order ridge segment, which results from regional mantle upwelling, concentration of sub-crustal magma along the axis and focused eruptions at the seafloor [e.g. Macdonald et al., 1984; Scheirer and Macdonald, 1994; Fornari et al., 1998; Haymon et al., 1991; 1993; Carbotte et al., 1997; Perfit and Chadwick, 1998]. The variability of the profiles shown in Figure 10B and distributions of sheet lava shown in Figures 8 and 9, may be the result of the localized, discontinuous overflow of lava from the ASCT along the eastern margin of the axial trough. The occurrence of sheet lava within an area dominated by lobate lava implies that the sheet lava is the product of discrete volcanic episodes separate from, and at higher effusion rates than those that produced the lobate lava. The mapped



concentration of sheet lava within the current center of volcanic activity may indicate a recent increase in eruptive effusion rate along this portion of the EPR crest.

Analysis of flow contacts (Table 4) suggests that the number of flow contacts is ~7 contacts per kilometer at distances <500 m off-axis and ~5 contacts per kilometer for distances >500 m off-axis. This apparent decrease in flow contacts at ~500 m off-axis could indicate a change in the eruptive dynamics of the ridge, and may coincide with the hypothetical increase in effusion rate. Variations in inferred lava ages (Figures 12 and 13) demonstrate the existence of multiple flow units along and across-axis. Although it is not possible to completely quantitatively define these lava flows with our data, the documentation of their existence and their variation in relative ages shows that the EPR crest out to ~1.5 km is an accumulation of multiple flow units which erupt not only from the axial trough but also from local eruptive centers located between ~ 500 - 2000 m from the ASCT. These flow units vary in age, lava morphology, emplacement distance from the ASCT, and possibly eruptive source [Perfit et al., 1994, 1995; Smith et al. 1997; Perfit and Fornari, unpublished data]; however, unless more complete coverage is obtained to better identify flow contacts and map out ridge crest flow units (ie high-frequency, near-bottom sidescan data), it will be difficult to fully address these questions.

A growing body of evidence indicates that off-axis volcanism, either by off-axis lava transport or eruption, does occur and potentially makes a significant volumetric contribution to the accumulation of the extrusive layer [e.g. Perfit et al., 1994; Perfit and Chadwick, 1998; Gregg et al., 1996; Macdonald et al., 1996; Goldstein et al., 1997; Sims et al., 1997]. Sheet lava, inferred to be significantly younger (~30 ka) than the crust upon which they are emplaced, have been documented ~1.5 km off-axis (Figure 13 : SH-1).

The photo-transect (SH-1) shown in Figure 13 suggests that these sheet lavas are an off-axis flow originating at or near the axial trough. Our suggestion that sheet flows within this region are a relatively recent product of an increased eruptive effusion rate at the axis supports this, and suggests that off-axis surface transport of axial lava is possible out to at least ~1.5 km from the ASCT.

Off-axis eruptions which can lead to emplacement of lobate flows from fissure eruptions or ridges of pillow lava [Perfit et al., 1994; Fornari et al., 1998; Cochran et al., 1996, submitted] act to thicken the crustal section away from the axis and may account for the formation of the benches in the broad crestal plateau east of the ASCT (Figures 9 and 10). Near-bottom gravity surveys of this region [Cochran et al., 1996; submitted] revealed Bouger anomalies of ~2-3 mGal over areas of observed pillow ridges, implying a focused eruptive source (i.e. a dike) below the pillow lava.

## **Conclusions**

Using the morphology and distribution of recent lava flows as mapped by photographic transects along the EPR crest between 9° 49' - 52'N (Figure 4), we examine volcanic processes over the zone of extrusive accumulation along this fast-spreading MOR for the past ~30 ka. Variation in ridge structure and distribution of the lava morphologies along and across the ridge crest support the hypothesis that off-axis volcanism contributes to the construction of young, fast-spreading ocean crust either through off-axis lava transport or off-axis eruptions. Our data suggest that the EPR crest has experienced at least three distinctly different types of volcanic emplacement processes.

(1) Summit eruptions within the near axis (<0.5 km) region are the principal means of volcanic construction at the ridge crest. The structure of the ridge crest, as deduced from multibeam bathymetric and near-bottom profiles, the relative percentages of volcanic morphologies, and the dominance and distribution of lobate lava suggest that for the past ~30 ka this 4th order segment of the EPR crest has experienced eruptions with similar effusion rates and volumes. No evidence was found for a large-scale eruption that had overprinted the seafloor like has been documented further south on the EPR crest near 9° 14-18'N [Wright et al., 1995a; Fornari et al., 1998]. The percentage and morphologic distribution of sheet lava (Figures 8 and 9) within the axial summit region and a conspicuous decrease in the number of flow contacts (Table 4) at ~500 m off-axis suggest that there has been a change in effusion style and perhaps an increase in eruptive effusion rate within the last ~10 ka in this area.

(2) Off-axis transport of lava erupted at or near the ASCT, either through lava tubes or surface flows [e.g. Haymon et al., 1993; Fornari et al., 1998], occurs to at least ~1.5 km off-axis and contributes to the accumulation of the extrusive oceanic layer. Three across-axis photo-transects (Figures 12 and 13) of lobate lava along the northern, middle, and southern sections of the survey region show the existence of multiple flow units of various ages and character, and support the data from the analysis of flow contacts (Table 4), suggesting that the ridge flank is built by the accumulation of multiple flows emplaced as discrete flow units throughout the region. A synoptic perspective of continuous high-frequency sonar imagery is needed to understand the regional and local contact relationships between lava flows.

(3) Off-axis extrusions including local constructional volcanism that creates small pillow ridges may account for the formation of a broad crestral plateau east of the ASCT. The correlation of young-looking pillow lava on low constructional ridges which also have 2-3 mGal Bouger anomalies [Cochran et al., 1996; submitted] with an off-axis crestral plateau, may indicate the existence of an off-axis eruptive center and would explain the build-up of a broad flat area east of the ASCT (Figure 10: #1 and #2). This process of off axis construction also helps explain how seismic layer 2A can thicken quickly near the axis of spreading.

All of these processes interact at different spatial and temporal scales along the crest of this 4th order MOR segment to form the upper oceanic crust. The region surveyed corresponds to the region over which crustal seismic layer 2A, believed to correspond to the extrusive oceanic layer, attains full thickness [Christeson et al., 1994, 1996; Hooft et al., 1996; Carbotte et al., 1997]. The regional percentages, a first order approximation of the number of flow units along the ridge crest, and the inferred relative ages of the lava morphologies suggest the contribution of off-axis volcanism to the accumulation of the upper oceanic extrusive layer is significant. Improved geologic mapping of the lava flows and the morphologic distributions along the ridge crest may allow us to begin a quantitative analysis of this contribution; however, such an effort will require high-resolution sidescan imagery, sampling and dating of flow units, and submersible observations of flow contacts. This type of high-resolution geologic mapping and quantitative analysis of the data are needed to improve our understanding of the growth and architecture of young oceanic crust at MORs.

## **Acknowledgments**

We thank our coPIs and the crews on the various Adventure dive programs: R. Haymon, M. Lilley, R. Lutz, M. Perfit, T. Shank, P. Shanks, and K. Von Damm for their cooperation in collecting the Mesotech data. Wyne Spencer provided invaluable help with the WHOI Camera System. This work was supported by National Science Foundation Grant: NSF-OCE-9100503 (DJF and MHE).

## APPENDIX A

### TABLES

Table 1. Alvin Dives with Bathymetry Data (1991-1995)

| Cruise  | Dates      | P-vent / Bio9 Dives | Marker 141 Dives    |
|---------|------------|---------------------|---------------------|
| Adv I   | Apr 91     | 2351 2357 2372      | -                   |
| Adv II  | Jan 92     | 2496 2501 2504      | -                   |
| Adv III | Dec 93     | 2692 2693           | 2690 2692 2693      |
| Adv IV  | Mar-Apr 94 | 2735 2743 2752 2758 | 2758                |
| Adv V   | Oct 94     | 2842 2846 2853      | 2844 2850 2852      |
| Adv VI  | Nov-Dec 95 | 3031 3033 3034 3035 | 3031 3033 3034 3035 |

Table 2. Lateral Shift Applied to Each Cruise

| Cruise  | Dates      | P-vent / Bio9 Data |         | Marker 141 Data |         |
|---------|------------|--------------------|---------|-----------------|---------|
|         |            | X shift            | Y shift | X shift         | Y shift |
| Adv II* | Jan 92     | 0 m                | 0 m     | 0 m             | 0 m     |
| Adv III | Dec 93     | +28 m              | -3 m    | +32 m           | +0 m    |
| Adv IV  | Mar-Apr 94 | +27 m              | +9 m    | +31 m           | +12 m   |
| Adv V   | Oct 94     | +27 m              | +1 m    | +31 m           | +4 m    |
| Adv VI  | Nov-Dec 95 | +14 m              | +8 m    | +14 m           | +13 m   |

\*AdvII cruise was used as baseline for all shifts

Table 3. Summary of Survey Line Analysis

| Times                             | Line Off-axis |           | Survey length (m) | Start Lat | Start Lon   | End Lat  | End Lon     | No. of images       | Feature Count & Percentage |     |          |     |        |    |
|-----------------------------------|---------------|-----------|-------------------|-----------|-------------|----------|-------------|---------------------|----------------------------|-----|----------|-----|--------|----|
|                                   | No.           | Dist (m)  |                   |           |             |          |             |                     | Fissures                   |     | Collapse |     | Faults |    |
| 2:51 - 3:30                       | 3a            | -         | -                 | 9.833401  | -104.285892 | 9.833522 | -104.286335 | 125                 | 0                          | 0%  | 5        | 4%  | 1      | 1% |
| 3:30 - 7:50                       | 3b            | 500 East  | 2087.00           | 9.833516  | -104.286325 | 9.851973 | -104.289800 | 1064                | 0                          | 0%  | 24       | 2%  | 4      | 0% |
| 2:05 - 7:51                       | 4             | 750 East  | 4557.68           | 9.862564  | -104.289549 | 9.822485 | -104.280831 | 1383                | 0                          | 0%  | 19       | 1%  | 5      | 0% |
| 1:24 - 7:14                       | 6             | 1500 East | 5732.29           | 9.866640  | -104.282469 | 9.815754 | -104.273993 | 1399                | 177                        | 13% | 21       | 2%  | 15     | 1% |
| 2:13 - 5:42                       | 9a            | 1000 East | 4059.14           | 9.863320  | -104.286727 | 9.827496 | -104.279584 | 836                 | 24                         | 3%  | 8        | 1%  | 1      | 0% |
| 5:42 - 7:42                       | 9b            | x         | 1529.87           | 9.827504  | -104.279597 | 9.827223 | -104.293361 | 480                 | 0                          | 0%  | 16       | 3%  | 0      | 0% |
| 7:42 - 8:02                       | 9c            | 500 West  | 390.53            | 9.827228  | -104.293354 | 9.830685 | -104.293988 | 80                  | 0                          | 0%  | 0        | 0%  | 0      | 0% |
| 4:34 - 7:30                       | 10a           | 0         | 3212.44           | 9.844982  | -104.293784 | 9.816673 | -104.287919 | 706                 | 0                          | 0%  | 380      | 54% | 0      | 0% |
| 7:30 - 7:48                       | 10b           | x         | 297.59            | 9.816660  | -104.287940 | 9.816757 | -104.290617 | 69                  | 0                          | 0%  | 62       | 90% | 0      | 0% |
| 7:48 - 10:23                      | 10c           | 250 West  | 3194.63           | 9.816778  | -104.290641 | 9.845214 | -104.294878 | 823                 | 1                          | 0%  | 250      | 40% | 0      | 0% |
| 10:10 - 10:35                     | A0a           | x         | 1122.75           | 9.835333  | -104.295151 | 9.844017 | -104.289986 | 101                 | 0                          | 0%  | 42       | 42% | 0      | 0% |
| 10:59 - 11:05                     | A0b           | 200 East  | 1064.34           | 9.835350  | -104.288132 | 9.843317 | -104.293449 | 31                  | 0                          | 0%  | 6        | 19% | 0      | 0% |
| 11:22 - 11:43                     | A0c           | x         | 828.22            | 9.837117  | -104.287697 | 9.841733 | -104.293549 | 85                  | 0                          | 0%  | 33       | 39% | 0      | 0% |
| 11:56 - 12:02                     | A0d           | 50 West   | 469.49            | 9.837383  | -104.292397 | 9.840700 | -104.289780 | 26                  | 0                          | 0%  | 12       | 46% | 0      | 0% |
| 12:29 - 12:46                     | A0e           | x         | 426.68            | 9.839050  | -104.293335 | 9.839167 | -104.289497 | 69                  | 0                          | 0%  | 45       | 65% | 0      | 0% |
| 12:46 - 12:52                     | A0f           | 100 East  | 352.73            | 9.839217  | -104.289299 | 9.838833 | -104.292450 | 26                  | 0                          | 0%  | 6        | 23% | 0      | 0% |
| 13:08 - 13:21                     | A0g           | x         | 486.21            | 9.841000  | -104.289780 | 9.837400 | -104.292267 | 55                  | 0                          | 0%  | 23       | 42% | 0      | 0% |
| 13:28 - 13:34                     | A0h           | 50 West   | 354.54            | 9.841817  | -104.293480 | 9.836900 | -104.287567 | 25                  | 0                          | 0%  | 9        | 36% | 0      | 0% |
| 13:46 - 14:00                     | A0i           | x         | 1056.67           | 9.843350  | -104.293404 | 9.835317 | -104.288315 | 55                  | 0                          | 0%  | 27       | 49% | 0      | 0% |
| 8:35 - 10:40                      | A1            | x         | 2869.49           | 9.831833  | -104.298416 | 9.832883 | -104.272614 | 324                 | 0                          | 0%  | 75       | 23% | 0      | 0% |
| 11:00 - 12:20                     | A2            | x         | 2141.72           | 9.867017  | -104.275917 | 9.866717 | -104.295189 | 504                 | 0                          | 0%  | 68       | 13% | 2      | 0% |
| <b>Along-axis (m) = 25622.08</b>  |               |           |                   |           |             |          |             | <b>No. Images =</b> | 8066                       |     |          |     |        |    |
| <b>Across-axis (m) = 10759.21</b> |               |           |                   |           |             |          |             |                     | 202                        | 3%  | 1130     | 14% | 28     | 0% |

| Line No.       | Morphology Count |    |      |    |     |    |     |     |     |       | Morphologic Percentage |    |      |    |     |    |     |     |     |       | Combined Percentage & Count |        |      |     |     |
|----------------|------------------|----|------|----|-----|----|-----|-----|-----|-------|------------------------|----|------|----|-----|----|-----|-----|-----|-------|-----------------------------|--------|------|-----|-----|
|                | 9                | 8  | 7    | 6  | 5   | 4  | 3   | 2   | 1   | Total | 9                      | 8  | 7    | 6  | 5   | 4  | 3   | 2   | 1   | Sheet | Lobate                      | Pillow |      |     |     |
| 3a             | 0                | 0  | 24   | 0  | 13  | 0  | 39  | 15  | 34  | 125   | 0%                     | 0% | 19%  | 0% | 10% | 0% | 31% | 12% | 27% | 70%   | 88                          | 19%    | 24   | 0%  | 0   |
| 3b             | 33               | 16 | 662  | 12 | 46  | 10 | 237 | 28  | 20  | 1064  | 3%                     | 2% | 62%  | 1% | 4%  | 1% | 22% | 3%  | 2%  | 27%   | 285                         | 62%    | 662  | 3%  | 33  |
| 4              | 335              | 51 | 728  | 12 | 26  | 18 | 176 | 1   | 36  | 1383  | 24%                    | 4% | 53%  | 1% | 2%  | 1% | 13% | 0%  | 3%  | 15%   | 213                         | 53%    | 728  | 24% | 335 |
| 6              | 171              | 9  | 1017 | 14 | 43  | 20 | 68  | 3   | 54  | 1399  | 12%                    | 1% | 73%  | 1% | 3%  | 1% | 5%  | 0%  | 4%  | 9%    | 125                         | 73%    | 1017 | 12% | 171 |
| 9a             | 141              | 2  | 584  | 9  | 8   | 16 | 52  | 0   | 24  | 836   | 17%                    | 0% | 70%  | 1% | 1%  | 2% | 6%  | 0%  | 3%  | 9%    | 76                          | 70%    | 584  | 17% | 141 |
| 9b             | 14               | 0  | 203  | 24 | 83  | 14 | 99  | 0   | 43  | 480   | 3%                     | 0% | 42%  | 5% | 17% | 3% | 21% | 0%  | 9%  | 30%   | 142                         | 42%    | 203  | 3%  | 14  |
| 9c             | 16               | 0  | 64   | 0  | 0   | 0  | 0   | 0   | 0   | 80    | 20%                    | 0% | 80%  | 0% | 0%  | 0% | 0%  | 0%  | 0%  | 0%    | 0                           | 80%    | 64   | 20% | 16  |
| 10a            | 1                | 2  | 547  | 2  | 18  | 1  | 25  | 89  | 21  | 706   | 0%                     | 0% | 77%  | 0% | 3%  | 0% | 4%  | 13% | 3%  | 19%   | 135                         | 77%    | 547  | 0%  | 1   |
| 10b            | 0                | 0  | 58   | 0  | 0   | 0  | 0   | 11  | 0   | 69    | 0%                     | 0% | 84%  | 0% | 0%  | 0% | 0%  | 16% | 0%  | 16%   | 11                          | 84%    | 58   | 0%  | 0   |
| 10c            | 4                | 1  | 555  | 2  | 0   | 0  | 6   | 8   | 27  | 603   | 1%                     | 0% | 92%  | 0% | 0%  | 0% | 1%  | 1%  | 4%  | 7%    | 41                          | 92%    | 555  | 1%  | 4   |
| A0a            | 1                | 0  | 83   | 0  | 0   | 0  | 1   | 3   | 13  | 101   | 1%                     | 0% | 82%  | 0% | 0%  | 0% | 1%  | 3%  | 13% | 17%   | 17                          | 82%    | 83   | 1%  | 1   |
| A0b            | 0                | 0  | 8    | 0  | 0   | 0  | 2   | 13  | 8   | 31    | 0%                     | 0% | 26%  | 0% | 0%  | 0% | 6%  | 42% | 26% | 74%   | 23                          | 26%    | 8    | 0%  | 0   |
| A0c            | 2                | 0  | 47   | 0  | 0   | 0  | 5   | 2   | 29  | 85    | 2%                     | 0% | 55%  | 0% | 0%  | 0% | 6%  | 2%  | 34% | 42%   | 36                          | 55%    | 47   | 2%  | 2   |
| A0d            | 0                | 0  | 22   | 0  | 0   | 0  | 0   | 2   | 2   | 26    | 0%                     | 0% | 85%  | 0% | 0%  | 0% | 0%  | 8%  | 8%  | 15%   | 4                           | 85%    | 22   | 0%  | 0   |
| A0e            | 0                | 0  | 51   | 0  | 0   | 0  | 1   | 4   | 13  | 69    | 0%                     | 0% | 74%  | 0% | 0%  | 0% | 1%  | 6%  | 19% | 26%   | 18                          | 74%    | 51   | 0%  | 0   |
| A0f            | 0                | 0  | 18   | 0  | 0   | 0  | 0   | 7   | 1   | 26    | 0%                     | 0% | 69%  | 0% | 0%  | 0% | 0%  | 27% | 4%  | 31%   | 8                           | 69%    | 18   | 0%  | 0   |
| A0g            | 0                | 0  | 55   | 0  | 0   | 0  | 0   | 0   | 0   | 55    | 0%                     | 0% | 100% | 0% | 0%  | 0% | 0%  | 0%  | 0%  | 0%    | 0                           | 100%   | 55   | 0%  | 0   |
| A0h            | 0                | 0  | 25   | 0  | 0   | 0  | 0   | 0   | 0   | 25    | 0%                     | 0% | 100% | 0% | 0%  | 0% | 0%  | 0%  | 0%  | 0%    | 0                           | 100%   | 25   | 0%  | 0   |
| A0i            | 1                | 0  | 53   | 0  | 0   | 0  | 1   | 0   | 0   | 55    | 2%                     | 0% | 96%  | 0% | 0%  | 0% | 2%  | 0%  | 0%  | 2%    | 1                           | 96%    | 53   | 2%  | 1   |
| A1             | 60               | 0  | 185  | 0  | 0   | 0  | 17  | 14  | 7   | 283   | 21%                    | 0% | 65%  | 0% | 0%  | 0% | 6%  | 5%  | 2%  | 13%   | 38                          | 65%    | 185  | 21% | 60  |
| A2             | 45               | 0  | 173  | 0  | 0   | 0  | 133 | 3   | 25  | 379   | 12%                    | 0% | 46%  | 0% | 0%  | 0% | 35% | 1%  | 7%  | 42%   | 161                         | 46%    | 173  | 12% | 45  |
| <b>Total =</b> | 824              | 81 | 5162 | 75 | 237 | 79 | 862 | 203 | 357 | 7880  | 10%                    | 1% | 66%  | 1% | 3%  | 1% | 11% | 3%  | 5%  | 18%   | 1422                        | 66%    | 5162 | 10% | 824 |

Pillow = 9      Lobate / Lineated = 6      Hackly Sheet = 3  
 Lobate / Pillow = 8      Hackly / Lobate = 5      Ropy Sheet = 2  
 Lobate = 7      Hackly / Lineated = 4      lineated Sheet = 1

Table 4. Summary of flow contact information for each towed camera survey line along the EPR crest 9° 49'-52' N.

|            | Dist<br>Off-axis | Length<br>(km) | Sediment Cover |       |     | Morphology |       |      | Lava Character |       |      |       | upper | lower | avg   | upper | lower | avg  |
|------------|------------------|----------------|----------------|-------|-----|------------|-------|------|----------------|-------|------|-------|-------|-------|-------|-------|-------|------|
|            |                  |                | upper          | lower | avg | upper      | lower | avg  | upper          | lower | avg  | Notes | Total | Total | Total | #/km  | #/km  | #/km |
| <b>10c</b> | -250             | 3.19           | 9              | 3     | 6   | 7          | 2     | 4.5  | 18             | 3     | 10.5 | 3     | 37.0  | 11.0  | 24.0  | 11.6  | 3.4   | 7.5  |
| <b>10a</b> | 0                | 3.21           | 10             | 3     | 6.5 | 9          | 3     | 6    | 13             | 3     | 8    | 2     | 34.0  | 11.0  | 22.5  | 10.6  | 3.4   | 7.0  |
| <b>3b</b>  | 500              | 2.09           | 10             | 3     | 6.5 | 12         | 2     | 7    |                |       |      | 1     | 23.0  | 6.0   | 14.5  | 11.0  | 2.9   | 6.9  |
| <b>4</b>   | 750              | 4.56           | 9              | 3     | 6   | 25         | 4     | 14.5 |                |       |      | 2     | 36.0  | 9.0   | 22.5  | 7.9   | 2.0   | 4.9  |
| <b>9a</b>  | 1000             | 4.01           | 9              | 3     | 6   | 19         | 3     | 11   | 1              | 1     | 1    | 2     | 31.0  | 9.0   | 20.0  | 7.7   | 2.2   | 5.0  |
| <b>6</b>   | 1500             | 5.73           | 21             | 5     | 13  | 25         | 4     | 14.5 |                |       |      | 2     | 48.0  | 11.0  | 29.5  | 8.4   | 1.9   | 5.1  |



APPENDIX B  
 FIGURES

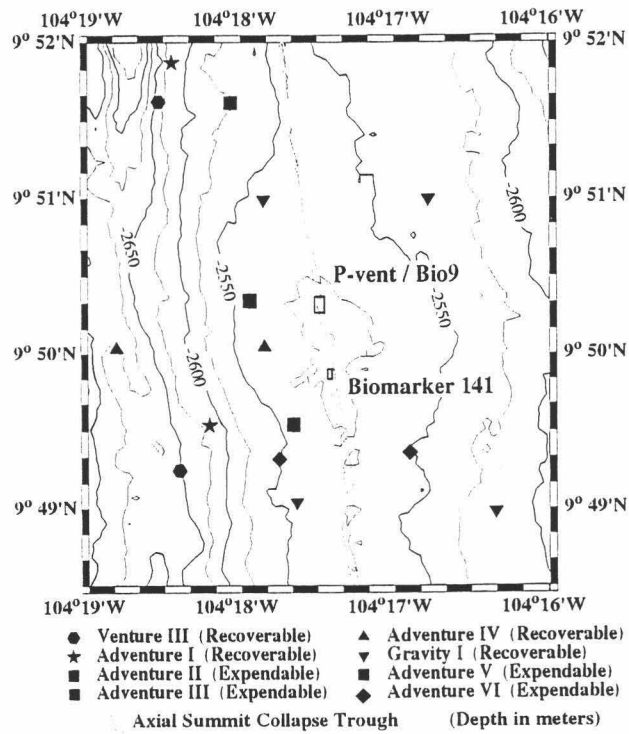


Figure 1. Bottom-moored acoustic transponders 1991-95. Transponders deployed in Mar. 1992 remained until Dec. 1995 providing consistent navigational references.

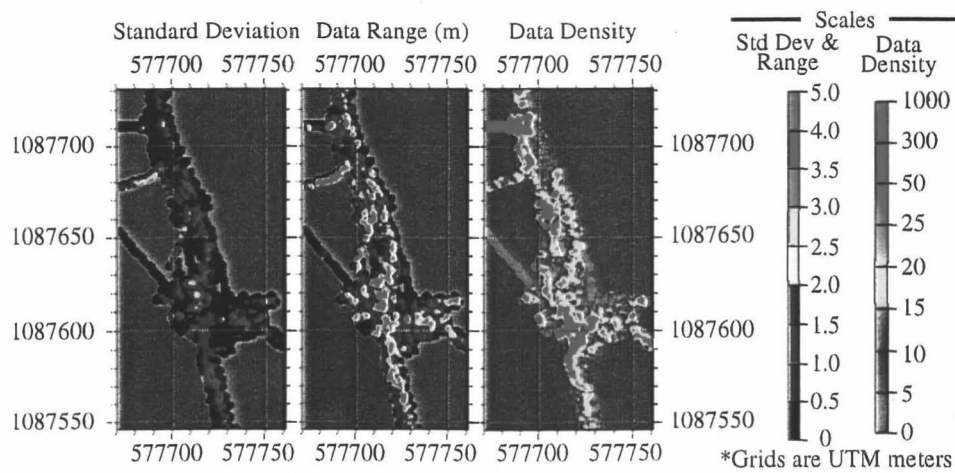


Figure 2. Statistical analyses of compiled 1995 bathymetry for the P-vent / Bio9 area located near 9° 50.3'N (Figure 1).

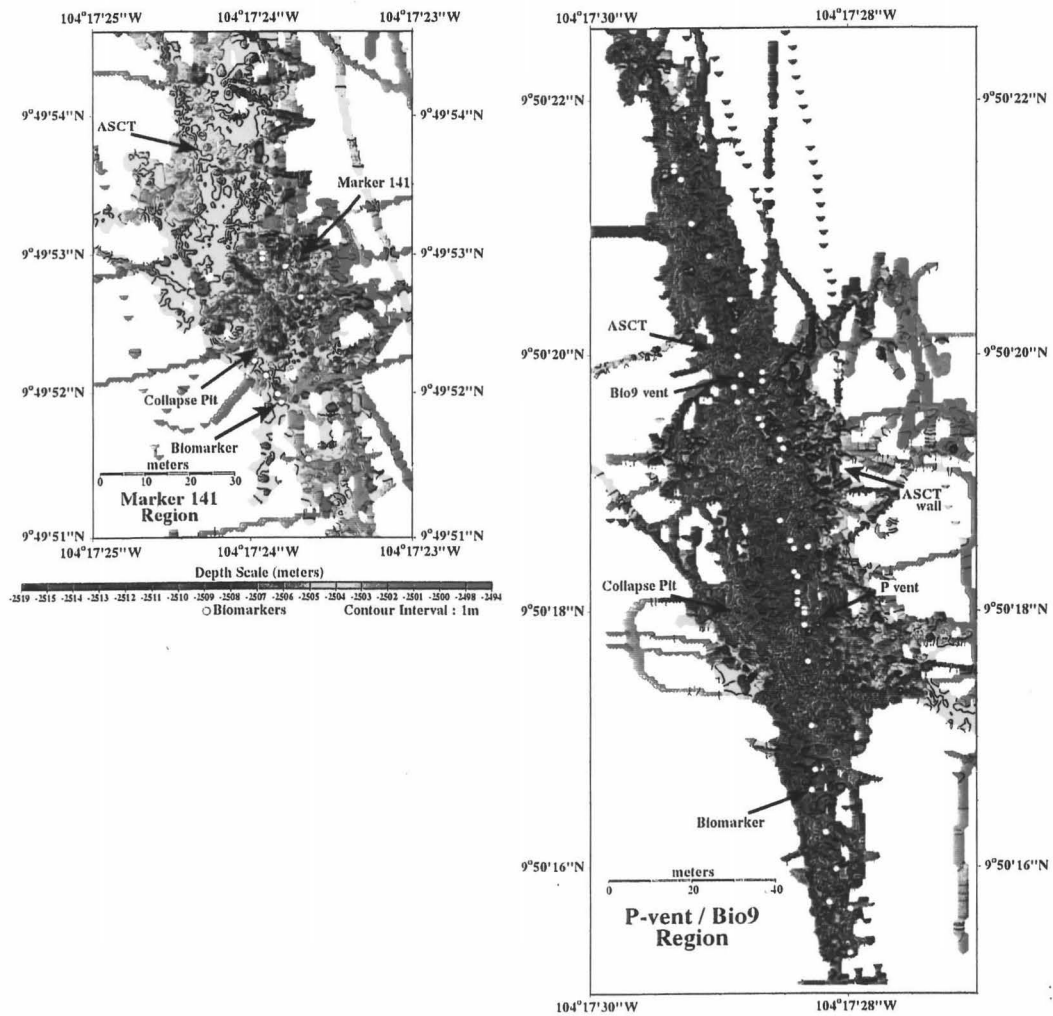


Figure 3. Bathymetric grids of P-vent / Bio9 and Biomarker 141 areas. Estimated data resolution is 5 m horizontal and 3 m vertical. Data represent the mean values of compiled and processed depth and altitude values recorded on 23 Alvin dives during dive programs that spanned 1991-95. The continuous linear color bar shows the color contour interval, along with a 1 m contour line interval. The white circles represent the Biomarkers placed on the ASCT floor for navigational reference. The scales of the maps are different and are shown within each image.

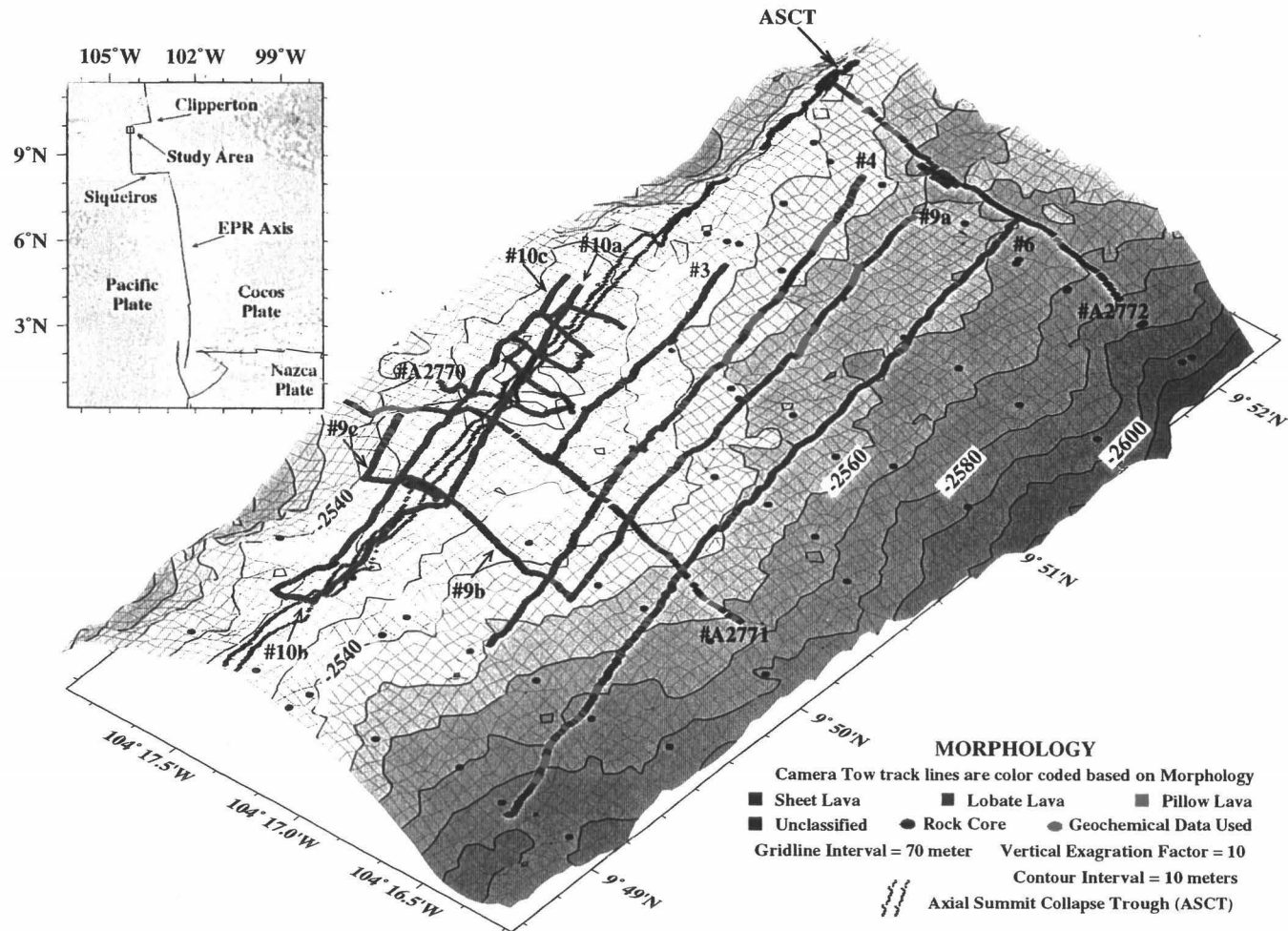


Figure 4. 3-D bathymetry model of the East Pacific Rise crest  $9^{\circ} 49' - 52' N$  showing locations of camera tows conducted in November, 1997, 1994 Alvin dive tracks, and rock core samples collected between 1993 and 1998. Multibeam bathymetry data collected in 1994 is contoured at 10 m intervals. Track lines are color coded to show lava morphology (see legend). Inset shows the location of study area with respect to plate boundaries in the eastern Pacific. To simplify analysis and presentation of data, three categories of "Lineated, Ropy, and Hackly" sheet lava are combined into a single "Sheet lava" category. The four "Hackly/Lineated, Hackly/Lobate, Lobate/Lineated, Lobate/Pillow" transitions or contact morphologies comprise ~6% of the total data set and are not shown on the bathymetry model or in Figure 9.



Figure 5. Photo-mosaic of a small lined sheet flow within a lobate terrain showing local-scale variations in flow morphology. At the lower left corner one can see a low relief (~0.5 m) collapse margin in the lobate flow which acted as a levee to contain the sheet flow. The surface glassiness of the two flows are equivalent suggesting that either the sheet flow was a late stage event in the same eruption that created the lobate flow, or is only slightly older, from a subsequent eruption. The right side of the sheet flow shows ropy textures suggesting vigorous movement of the flow surface as it spilled over the lobate lava along this edge. The top of the mosaic (the down hill and westward edge of the flow) shows a transition of the sheet flow from a lined to a hackly surface, formed as the flow lost velocity and spilled out of the contained channel. These types of very localized transitions point to the important effects which effusion rate and local pre-flow topography have in controlling submarine lava flow morphology. The flow is ~ 6 m wide by 17 m in length, and is located ~300 m west of the ASCT running from east to west (Figure 9).

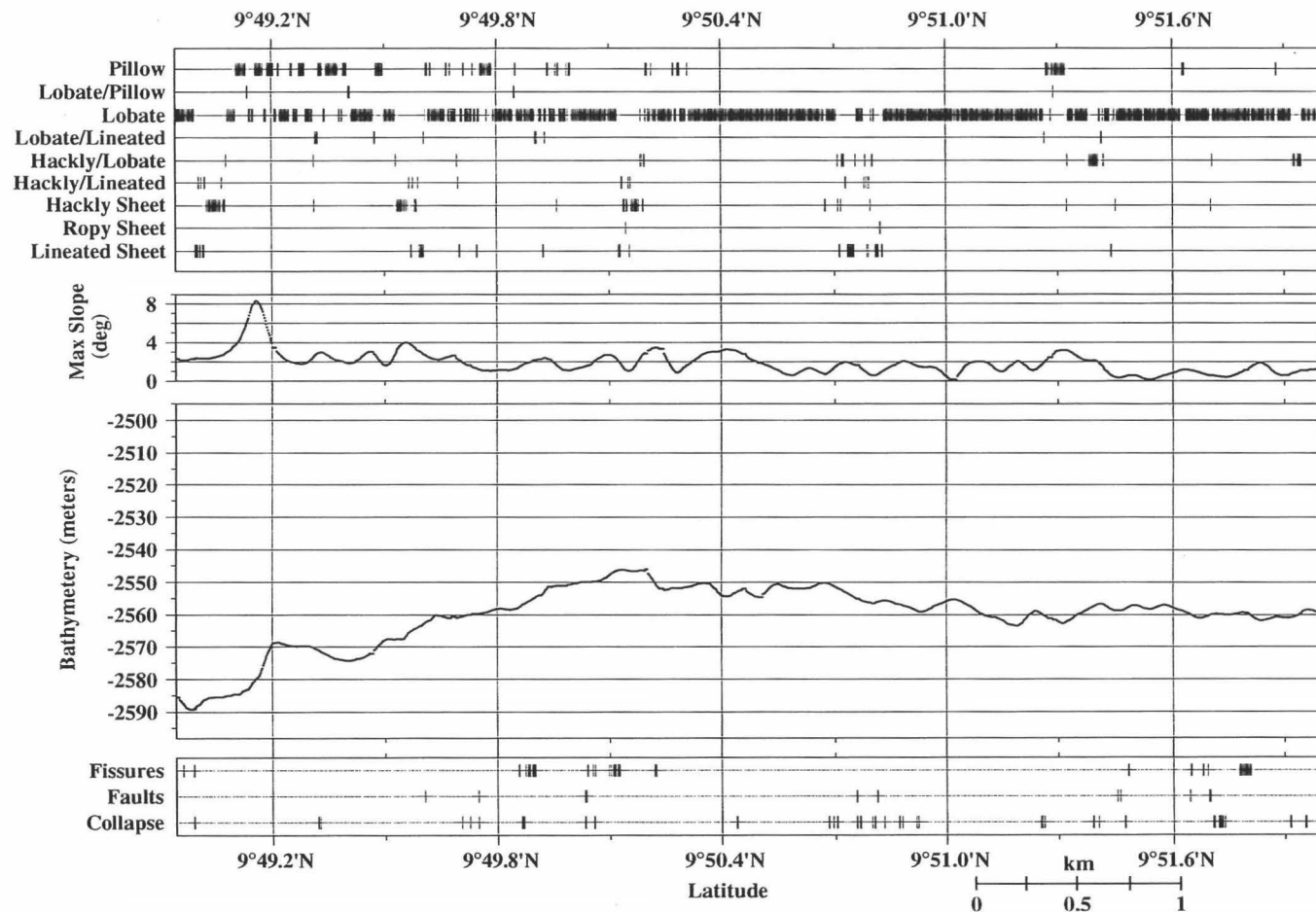


Figure 6. Example of image analysis performed on data from each camera survey line and Alvin dive shown in Figure 1. Each image was classified into one of five main or four transitional categories of lava morphology, and assigned a slope and depth based on location and correlation to 1994 multibeam data. The occurrence of geologic features such as fissures, faults, and collapse was also noted. Displaying the summary of each survey line in this manner allowed us to examine relationships between morphology, slope, and terrain. Plotting the different morphologies in a geographic reference frame (top panel) we looked for repeated patterns in lava transitions. The distance between each vertical latitude line is 1.11 km ( $0.6' \text{ lat} = 1.11 \text{ km}$ ).

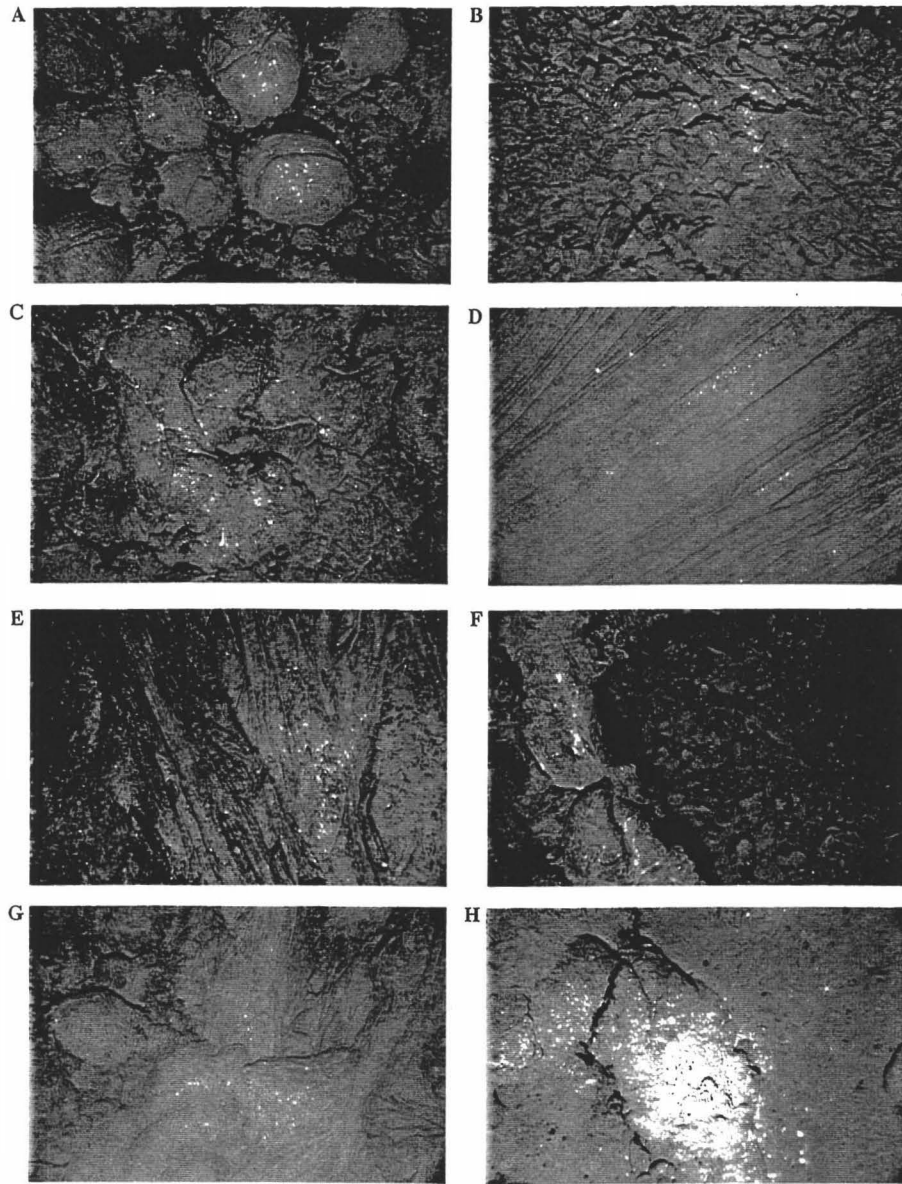


Figure 7. Digital photographs showing differences in lava glassiness, sediment cover and infilling between forms, and lava surface texture, as well the different volcanic morphologic categories and features used to analyze and classify the seafloor on the East Pacific Rise crest between  $9^{\circ} 49' - 52' \text{ N}$ . (a) Pillow lava. (b) Hackly lava. (c) Lobate lava. (d) Lineated sheet lava. (e) Ropy sheet lava. (f) Collapse feature ( $\sim 1\text{m}$  in depth). (g) A contact between lobate lava (foreground) and underlying sheet lava (top of photo). (h) Heavily sediment-covered lobate flow with a small ( $\sim 6 \text{ cm}$ ) fissure running across the extrusive form. The scale of the images ranges from  $2 \text{ m} \times 3 \text{ m}$  to  $4 \text{ m} \times 6 \text{ m}$ , depending upon the altitude of the camera system. As we do not have a record of distance off bottom, images scales are only approximations.

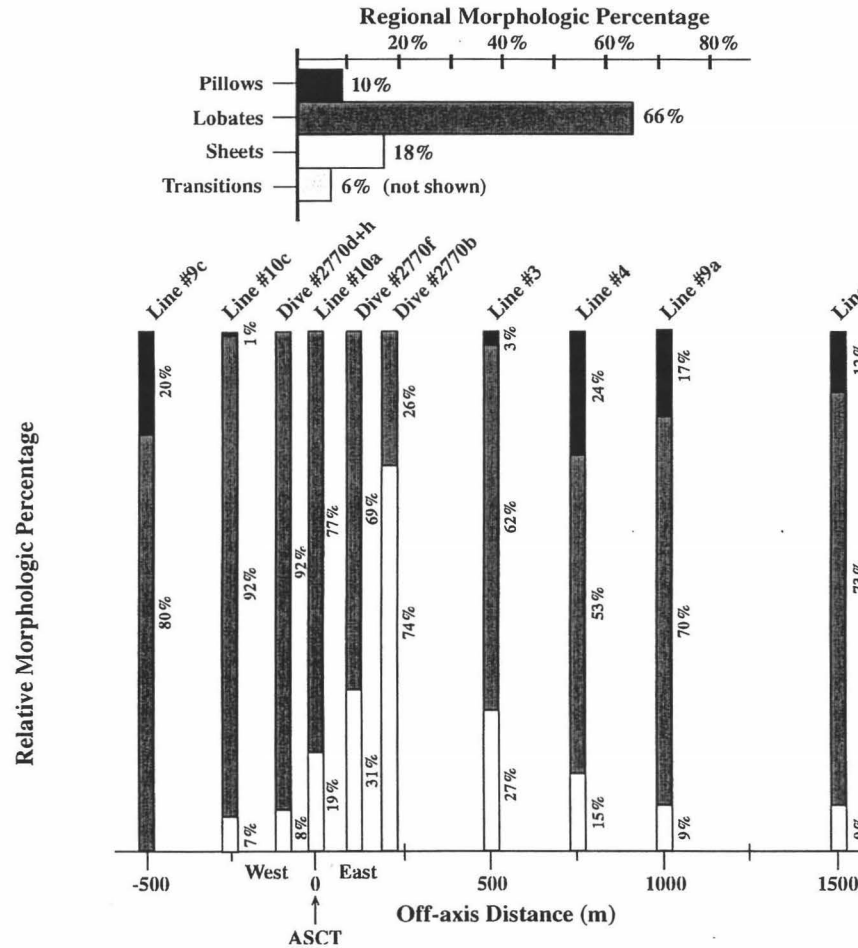


Figure 8. Relative distribution of lava morphologies using data from each camera tow line across the East Pacific Rise (EPR) axis over the survey area shown in Figure 1. Histogram at top of figure shows overall regional percentage of each lava morphology from camera tow and Alvin dive data. Lobate lava dominates the EPR crest between  $9^{\circ} 49' N$  and  $9^{\circ} 52' N$ . Percentages in main figure next to vertical bars show relative percent of each lava morphology along individual survey line segments. These percentages have not been normalized to the length of each survey line, and therefore do not reflect region morphologic distributions. Line numbers refer to tracks shown in Figure 4, and colors are keyed to the histogram. Lower plot illustrates that sheet lava are focused near the ridge axis, while pillow lava are concentrated at distances  $\sim 500$  m from the ridge axis.



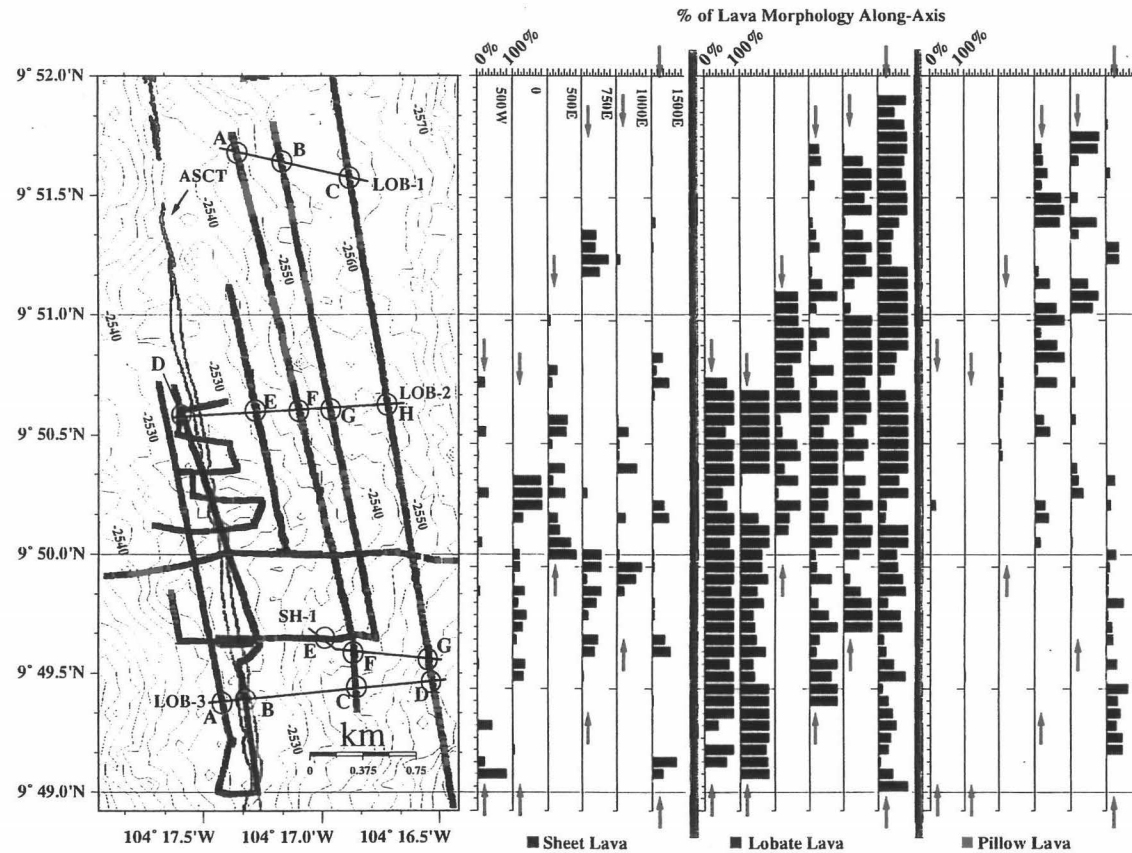


Figure 9. Distribution of lava morphology for each along-axis survey line at a fixed distances from the axial summit collapse trough (ASCT) [Fornari et al., 1998]. Camera tow and Alvin survey lines are color coded to morphology as in Figure 1 and plotted on Seabeam bathymetry contoured at a 10 m intervals. The ASCT is shown as a dark line along the ridge axis. Percentages shown were calculated from the morphologies contained in consecutive along-axis 100 m segments for each survey line. Percentages of sheet, lobate, and pillow lava were separated into a single panel for each morphology and plotted versus latitude corresponding to the bathymetry map shown at left. Arrows at ends of each percentage plot indicate extent of the area surveyed. These morphologic percentages and their distributions show that sheet lava are principally concentrated around the axial summit high; however, sites of sheet lava deposition are present as far as 1.5 km from the ASCT and in most instances these lava are younger than the lobate lava they are in contact with. Pillow lava are more prevalent at distances >0.5 km from the ASCT and appear to be concentrated more in the northern half of the surveyed area. Thick black lines labeled LOB-1, LOB-2, LOB-3, and SH-1 represent photo-transects shown in Figures 12 and 13. The letters on each photo-transect line correspond to the letters identifying individual images in Figures 12 and 13.

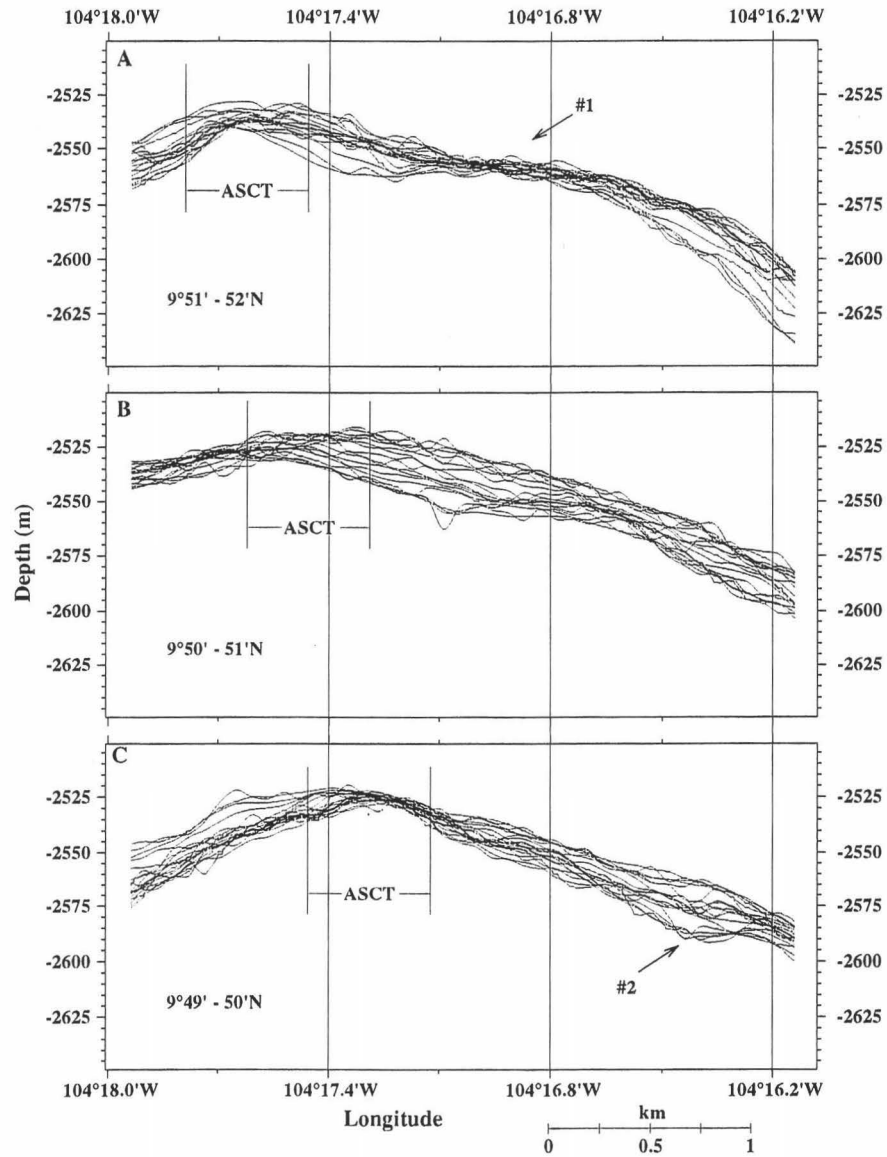


Figure 10. Across-axis bathymetry profiles calculated from the 1994 Seabeam bathymetry data every 100 m along-axis and compiled into three sections representing the northern [9° 51' - 52' N], middle [9° 50' - 51' N], and southern [9° 49' - 50' N] regions of the study area. These data show the local-scale variation in the ridge crest structure along the EPR axis which, in a broad sense, correlates to the distribution of volcanic morphologies mapped using the towed camera data. The minimum slope and maximum cross-sectional area [Scheirer and Macdonald, 1993] are located near the axial summit high (~9°50.3' N) which is in the middle panel.

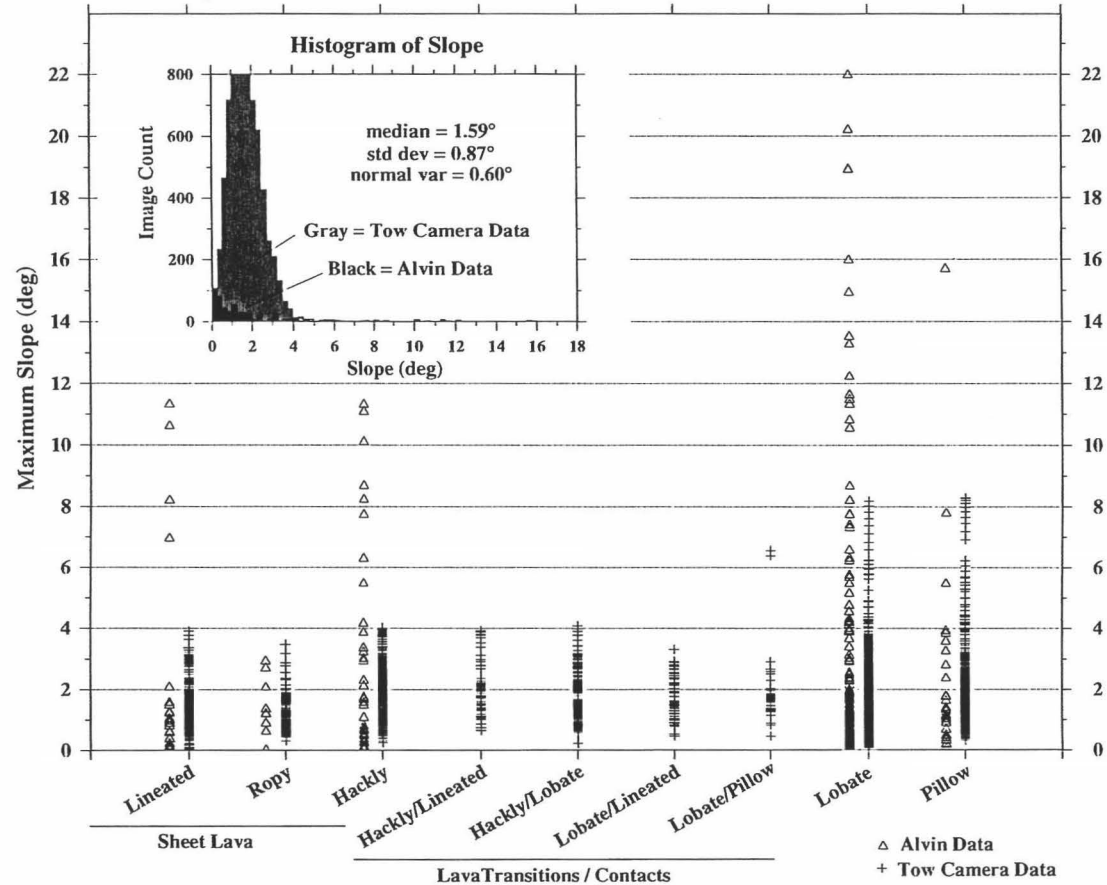


Figure 11. Lava morphology plotted as a function of regional topographic slope (as calculated from the 1994 Seabeam data) to demonstrate the range of morphologies deduced from the towed camera data occur over the entire range of slopes. All of the morphologic types of lava forms are seen over the 0° - 4° range (99% of the region) of calculated slope angle, indicating that topographic slope is not the dominant controlling factor, but only one of many factors determining lava morphology. We caution that these slope measurements were made based on 50 m gridded Seabeam data and not near-bottom profiles which could account for the homogenization of the slope values to all the volcanic morphologies. Detailed near-bottom profiles were not possible on the camera tows because the altimeter was not functioning. Future work using this system should ensure that the altimeter is working. Inset histogram shows the distribution of slope angles for the entire survey area shown in Figure 1 based on a single slope value for each digital image collected. This distribution of slope angles indicates that the local gradient of the EPR crest at the 4th-order segment scale is ~1.6°.

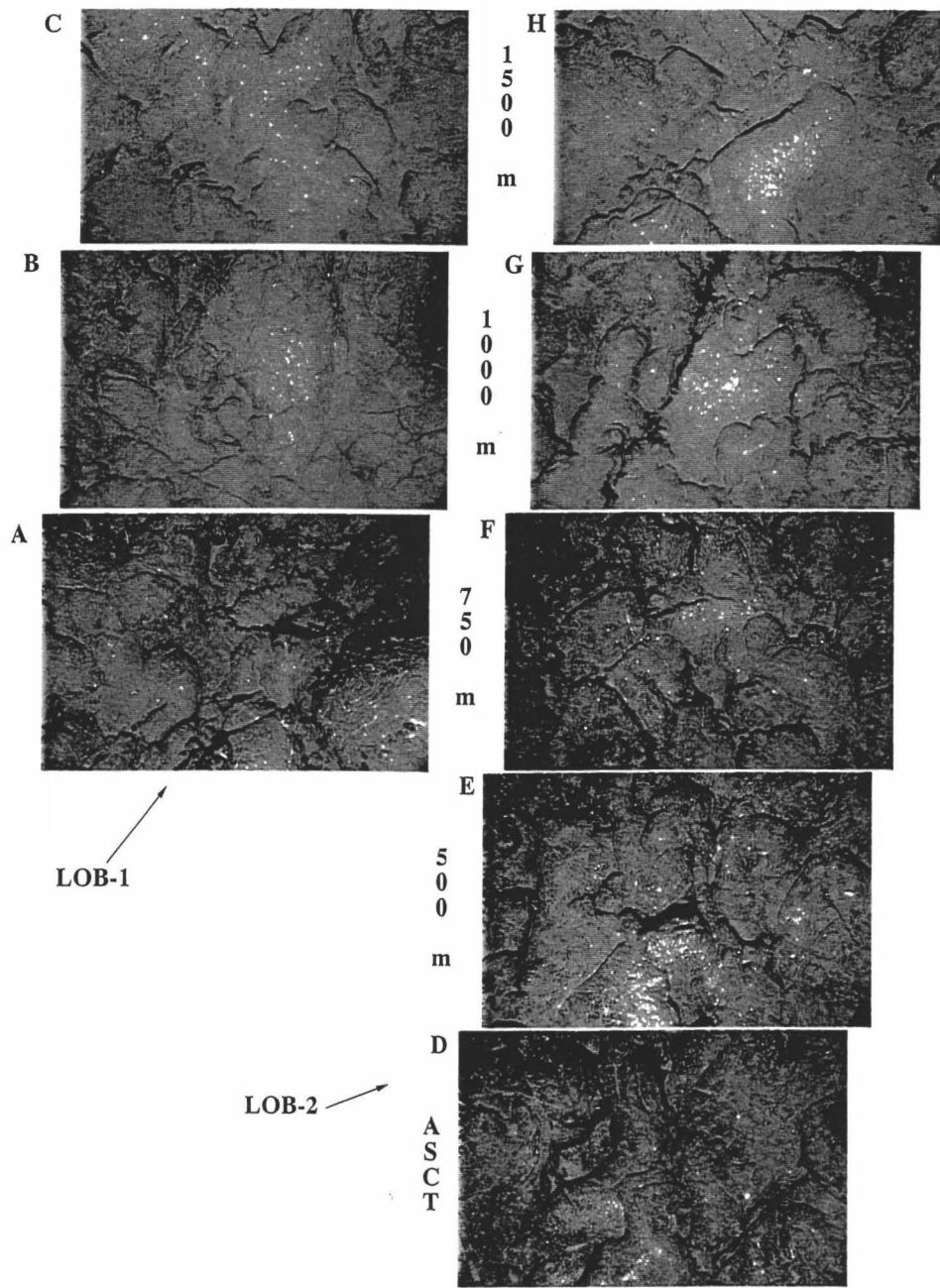


Figure 12. Photo-transects (LOB-1 & LOB-2) over areas of lobate lava across-axis at  $\sim 9^{\circ}51.5'N$  and  $9^{\circ}50.5'N$  (see Figure 9 for transect locations) showing the inferred relative ages of lava increasing with distance from the ASCT and variability in lobate forms. As distance off-axis increases, sediment infill between the lava forms increases, sediment cover increases, surface texture becomes rougher, and the glassiness of the lava decreases. Contrasting LOB-2 (D), an image within the ASCT, with LOB-2 (H), an image 1.5 km off-axis, these changes are apparent. At distances of 1.0 - 1.5 km off-axis, tectonic features such as cracks and faults, shown in LOB-2 (G), become more frequent. The scale of each image is  $\sim 4 \text{ m} \times 6 \text{ m}$ .

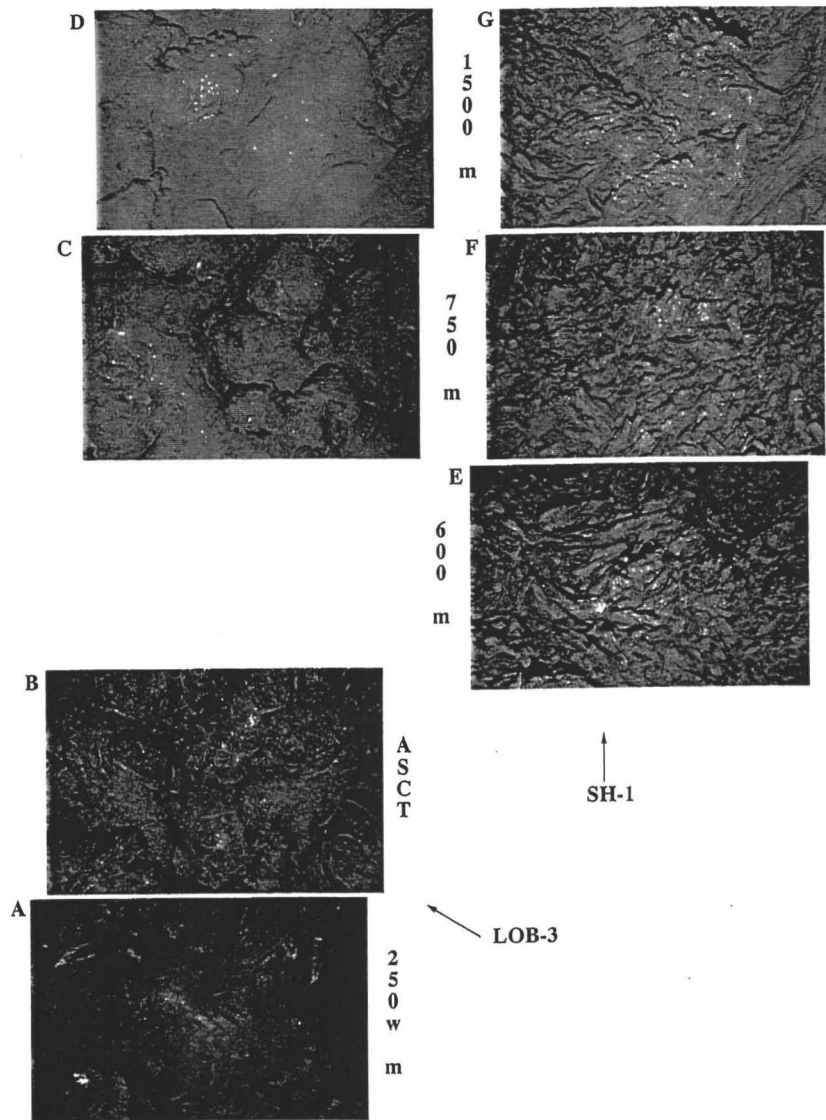


Figure 13. Across-axis photo-transects (LOB-3 & SH-1) of a lobate lava and sheet lava near 9°49.5'N (see Figure 9). Photographs in LOB-3 transect show changes in lava glassiness and luster (inferred age) with increasing distance from the ASCT. LOB-3 (A) is located 250 m west of the ASCT and is believed to be a product of the 1991 or 1992 eruption. LOB-3(B) is also a very glassy, fresh looking lava imaged in the ASCT and is likely to be a product of the 1991-1992 eruptions [Haymon et al., 1993, Rubin et al. 1994]. The inferred age differences between LOB-3 (A) 250 m west of the ASCT and LOB-3 (D) 1.5 km east of the axis are obvious. Photo-transect SH-1 demonstrates the similar surface texture and apparent lack of sediment cover on hackly sheet flows located 0.60 km, 0.75 km, and 1.5 km off-axis. Although these sheet lava were emplaced upon crust with presumed magnetic age differences of ~10-15 ka, it is difficult to distinguish an age difference between the hackly lava of SH-1 which covers an across-axis distance of ~1000 m. LOB-3 (D) and SH-1 (G) are both 1.5 km east of the ASCT and are located only ~300 m apart (Figure 6). While not conclusive because of the lack of photo-coverage (see Figures 1 and 6), the data suggest that this particular sheet flow may have originated at the ASCT and flowed at least ~1500 m from the axis and as such may be ~30ka younger than the crust upon which it is emplaced. The scale of each image is ~4m x 6m.

## REFERENCES

- Ballard, R.D., and T.H. Van Andel, Morphology and tectonics of the inner rift valley at lat 36°50'N on the mid-Atlantic ridge, *Geol. Soc. of America Bull.*, 88, 507-530, 1977
- Ballard, R. D., R. T. Holcomb, and T. H. van Andel, The Galapagos Rift at 86°W, sheet flows, collapse pits, and lava lakes of the rift valley, *J. Geophys. Res.*, 84, 5407-5422, 1979.
- Ballard, R. D., J. Francheteau, T. Juteau, C. Rangan, and W. Normark, EPR at 21°N: Volcanic, tectonic and hydrothermal processes of the central axis, *Earth Planet. Sci. Lett.*, 55, 1-10, 1981.
- Ballard, R. D., and J. Francheteau, the relationship between active sulfide deposition and the axial processes of the mid-ocean ridge, *Mar. Technol. Soc. J.*, 16, 8-20, 1982.
- Ballard, R. D., R. Hekinian, and J. Francheteau, Geological setting of hydrothermal activity at 12°50'N on the East Pacific Rise: A submersible study, *Earth Planet. Sci. Lett.*, 69, 176-186, 1984.
- Bonatti, E., and C.G. Harrison, Eruption styles of basalt in oceanic spreading ridges and seamounts: effect of magma temperature and viscosity, *J. Geophys. Res.*, 93, B4, 2967-2980, 1988;
- Carbotte, S., and K. C. Macdonald, East Pacific Rise 8°N-10°30'N: Evolution of ridge segments and discontinuities from SeaMARC II and three-dimensional magnetic studies, *J. Geophys. Res.*, 97, 6959-6982, 1992.
- Carbotte, S. M. and K. C. Macdonald, The axial topographic high at intermediate and fast spreading ridges: *Earth and Planet. Sci. Lett.*, 128, 85-98, 1994.
- Carbotte, S.M., J.C. Mutter, L. Xu, Contribution of volcanism and tectonism to axial and flank morphology of the southern EPR, 17°10'-17°40'S, from a study of Layer 2A geometry, *J. Geophys. Res.*, in press 1997
- Chadwick, W.W., Jr., R.W. Embley, and C.J. Fox, SeaBeam depth changes associated with recent lava flows, CoAxial segment, Juan de Fuca Ridge: Evidence for multiple eruptions between 1981-1993, *Geophys. Res. Lett.*, 22, 167-170, 1995.
- Chadwick, W. W., Jr., and R. W. Embley, Lava flows from a mid-1980s submarine eruption on the Cleft Segment, Juan de Fuca Ridge, *J. Geophys. Res.*, 99, 4761-4776, 1994.
- Christeson, G.L., G.M. Purdy, and G.L. Fryer, Structure of young oceanic crust at the East Pacific Rise near 9°30'N, *Geophys. Res. Lett.*, 19, 1045-1048, 1992.
- Christeson, G. L., G. M. Purdy, and G. J. Fryer, Seismic constraints on shallow crustal emplacement processes at the fast spreading East Pacific Rise, *J. Geophys. Res.*, 99, 17,957-17,974, 1994a.
- Christeson, G. L., W.S.D. Wilcock, and G.M. Purdy, The shallow attenuation structure of the fast spreading East Pacific Rise near 9°30'N, *Geophys. Res. Lett.*, 21, 321-324, 1994b.
- Christesen, G.L., G.M. Kent, G.M. Purdy and R.S. Detrick, Extrusive thickness variability at the East Pacific Rise, 9° -10°N: Constraints from seismic techniques, *J. Geophys. Res.* 101, 2859-2873, 1996.

- Christeson, G. L., Shaw, P. R., Garmany, J. D., Shear and compressional wave structure of the East Pacific Rise, 9°-10° N, *Journal of Geophysical Research*, B, Solid Earth and Planets, 102 (4), 7821-7835, 1997
- Cochran, J. R., D. J. Fornari, B. J. Coakley, and R. Herr, Near-bottom underway gravity study of the shallow structure of the axis of the East Pacific Rise, 9° 31'N and 9° 50'N, *Eos Trans. AGU*, 77 (46), Fall Meet. Suppl., F698, 1996.
- Cochran et al. (Continuous near-bottom gravity measurements made with a BGM-3 gravimeter in DSV *Alvin* on the East Pacific Rise crest 9°30' and 9°50'N, submitted to *Journal of Geophysical Research*, 1997
- Dziak, R.P., C.G. Fox and A.E. Schreiner, The June-July seismo-acoustic event at CoAxial Segment, Juan de Fuca Ridge, *Geophys. Res. Letts.*, 22, 135-138, 1995.
- Edwards, M. H., D. J. Fornari, T. A. O'Brien and R. M. Haymon, High-resolution ARGO sonar data for the EPR crest 9°-10°N: Implications for ridge crest processes, *Eos Trans. AGU*, 71(17), 621, 1990.
- Edwards, M. H., D. J. Fornari, A. Malinverno, W. B. F. Ryan and J. Madsen, The regional tectonic fabric of the East Pacific Rise from 12°50'N to 15°10'N, *J. Geophys. Res.*, 96, 7995-8017, 1991.
- Embley, R.W., and W.W. Chadwick, Volcanic and hydrothermal processes associated with a recent phase of seafloor spreading at the northern Cleft segment: Juan de Fuca Ridge, *J. Geophys. Res.*, 99, 4741-4760, 1994.
- Embley, R. W., W. W. Chadwick Jr., I. R. Jonasson, D. A. Butterfield, and E. T. Baker, Initial results of the rapid response to the 1993 CoAxial event: Relationships between hydrothermal and volcanic processes, *Geophys. Res. Lett.*, 22, 143-146, 1995.
- Embley, R. W., W. W. Chadwick Jr., T. Shank, and D. Christie, Geology of the 1996 Gorda Ridge eruption from analysis of multibeam, towed camera, sidescan, and ROV data, *Eos Transactions of the American Geophysical Union*, 77, 1996.
- Fornari, D.F., and R.W. Embley, Tectonic and volcanic controls on hydrothermal processes at the mid-ocean ridge: an overview based on near-bottom and submersible studies, in *Seafloor Hydrothermal Systems*, edited by J. Lupton, L. Mullineaux, R. Zierenberg, and R. Thompson, pp. 1-46, AGU, Washington, D.C., 1995.
- Fornari, D.J., Haymon, R. M., Perfit, M. R., Gregg, T.K.P., Edwards, M. H., Geological Characteristics and Evolution of the Axial Zone on Fast Spreading Mid-Ocean Ridges: Formation of an Axial Summit Trough along the East Pacific Rise, 9° -10° N, *J. Geophys. Res.*, (in press), 1998.
- Fox, C.G, W.W. Chadwick, and R.W. Embley,. Detection of Changes in Ridge-Crest Morphology Using Repeated Multibeam Sonar Surveys, *J. Geophys. Res.*, 97, B7, 11149-11162, Jul 1992
- Fox, C. G., H. Matsumoto, and T-K. Lau, Monitoring East Pacific Rise seismicity using autonomous hydrophone moorings, *Trans. American Geophys. U.*, EOS, 78, F705, 1997.
- Fox, C.G., and R.P. Dziak, Sesimo-acoustic detection of volcanic activity on the Gorda Ridge, February-March, 1996, *Trans. American Geophys. U.*, EOS, F-1, 1996.
- Fox, C. G., and R. P. Dziak, Hydroacoustic detection of volcanic activity on the Gorda Ridge, February-March, *Deep-Sea Res.*, in press 1998

- Francheteau, Jean, Ballard, Robert D., The East Pacific Rise near 21 degrees N, 13 degrees N and 20 degrees S; inferences for along-strike variability of axial processes of the mid-ocean ridge, *Earth and Planetary Science Letters*, 64(1), p. 93-116, 1983.
- Gente, P., J.M. Auzende, V. Renard, Y. Fouquet and D. Bideau, Detailed geological mapping by submersible of the East Pacific Rise axial graben near 13°N, *Earth Planet. Sci. Letts.*, 78, 224-236, 1986.
- Griffiths, R.W., J.H. Fink, Solidification and morphology of submarine lavas: A dependence on extrusion rate, *J. Geophys. Res.*, 97, 19729-19737, 1992
- Gregg, T.K.P., J.H. Fink, Quantification of submarine lava-flow morphology through analog experiments, *Geology*, 23, 73-76, 1995
- Gregg, T.K.P., D.J. Fornari, M.R. Perfit, M.R. Haymon, J.H. Fink, Rapid emplacement of a mid-ocean ridge lava flow on the East Pacific Rise at 9°46'-51'N, *Earth Planet. Sci. Lett.* 144, E2, 1996a
- Gregg, T.K.P., D.J. Fornari, M.R. Perfit, 1996b, Lava Pillars: "Rosetta stones" of deep sea eruption dynamics, *EOS Trans. AGU*, 77, F664.
- Gregg, T.K.P. and W.W. Chadwick, Jr., Submarine lava-flow inflation: A model for the formation of lava pillars, *Geology*, 23, 73-76, 1996.
- Gregg, T.K.P., and L.P. Keszthelyi, The emplacement of Pahoehoe toes: Field observations and comparison to laboratory simulations, *Bull. Of Volcanology*, submitted, 1998
- Harding, A. J., G. M. Kent, and J. A. Orcutt, A multichannel seismic investigation of the upper crustal structure at 9° N on the East Pacific Rise: Implications for crustal accretion, *J. Geophys. Res.*, 98, 13,925-13,944, 1993.
- Haymon R.M., D.J. Fornari, M.H. Edwards, S. Carbotte, D. Wright, and K.C. Macdonald, Hydrothermal vent distribution along the East Pacific Rise Crest (9° 09'-54'N) and its relationship to magmatic and tectonic processes on fast-spreading mid-ocean ridges, *Earth Planet. Sci. Lett.*, 104, 513-534, 1991.
- Haymon, R.M., D.J. Fornari, K.L. Von Damm, M.D. Lilley, M.R. Perfit, J.M. Edmond, W.C. Shanks III, R.A. Lutz, J.M. Grebmeier, S. Carbotte, D. Wright, E. McLaughlin, M. Smith, N. Beedle and E. Olson, Volcanic eruption of the mid-ocean ridge along the EPR crest at 9° 45-52'N: Direct submersible observations of seafloor phenomena associated with an eruption event in April, 1991, *Earth Planet. Sci. Lett.*, 119, 85-101, 1993.
- Haymon, R. M., 1996, The response of ridge crest hydrothermal systems to segmented, episodic magma supply, in: *Tectonic, Magmatic and Hydrothermal and Biological Segmentation of Mid-Ocean Ridges*, eds.: C.J. McLeod, P.A. Tyler, and C.L. Walker, *Geological Society of London Special Publication*, 118, 157-168, 1996.
- Hon, K., J. Kauahikaua, R. Denlinger, K. Mackay, Emplacement and inflation of pahoehoe sheet flows: Observations and measurements of active lava flows on Kilauea volcano, Hawaii, *Geol. Soc. of America Bull.*, 106, 351-370, 1994
- Hooft, E.E.E., H. Schouten, and R.S. Detrick, Constraining crustal emplacement processes from the variation of seismic layer 2A thickness at the East Pacific Rise, *Earth Planet. Sci. Lett.* 142, 289-310, 1996
- Hulme, G., The interpretation of lava flow morphology, *Geophys. J. Res. Astr. Soc.*, 39, 361-383, 1974



- Kurras, G.J., M.H. Edwards, D.J. Fornari, High-resolution bathymetry of the East Pacific Rise axial summit trough 9° 49'-51' N: A compilation of *Alvin* scanning sonar and altimetry data from 1991-1995, *Geophys. Res. Lett.*, 1998
- Langmuir, C.H., J.F. Bender and R. Batiza, Petrologic and tectonic segmentation of the East Pacific Rise, 5°30'-14°30'N, *Nature*, 322, 422-429, 1986.
- Laughton, A. S., and Searle, R. C., Tectonic processes on slow spreading ridges, *Maurice Ewing Series*, 2, 15-32, 1979
- Lonsdale, P. F., Structural geomorphology of a fast-spreading rise crest: The East Pacific Rise near 3°25'S: *Mar. Geophys. Res.*, v. 3, p. 251-293, 1977.
- Lonsdale, Peter, Linear volcanoes along the Pacific-Cocos plate boundary, 9°N to the Galapagos triple junction, *Tectonophysics*, 116 (3-4), p. 255-279
- Macdonald, K., J.-C. Sempere and P. J. Fox, 1984, East Pacific Rise from Siqueiros to Orozco Fracture Zones: Along-strike continuity of axial neovolcanic zone and structure and evolution of overlapping spreading centers: *J. Geophys. Res.*, 89, 6049-6069, 1984.
- Macdonald, K. C. and P. J. Fox, The axial summit graben and cross-sectional shape of the East Pacific Rise as indicators of axial magma chambers and recent volcanic eruptions: *Earth Planet. Sci. Lett.*, v. 88, 119-131, 1988.
- Macdonald, K. C., P. J. Fox, S. Carbotte, M. Eisen, S. Miller, L. Perram, D. Scheirer, S. Tighe and C. Weiland, The East Pacific Rise and its flanks, 8°-17° N: History of segmentation, propagation and spreading direction based on SeaMARC II and Sea Beam studies: *Mar. Geophys. Res.*, 14, 299-344, 1992.
- Macdonald, K.C., P.J. Fox, R.T. Alexander, R. Pockalny, P. Gente, Volcanic growth faults and the origin of abyssal hills on the flanks of the East Pacific Rise, *Nature*, 380,125-129, 1996
- McConachy, T. F., R. D. Ballard, M. J. Mottl and R. P. von Herzen, Geologic form and setting of a hydrothermal vent field at 10°56'N, East Pacific Rise: A detailed study using ANGUS and *Alvin*, *Geology*, 14, 295-298, 1986.
- Malin, M.C., Lengths of Hawaiian lava flows, *Geology*, 8, 306-308, 1980
- Moore, J.G., Mechanism of formation of pillow lava, *American Scientist*, 63, 3, 269-277, 1975
- Perfit, M.R., D.J. Fornari, M.C. Smith, J.F. Bender, C.H. Langmuir, R.M. Haymon, Small-scale spatial and temporal variations in mid-ocean ridge crest magmatic processes, *Geology*, 22, 375-379, 1994
- Perfit, M. R., M. C. Smith, K. Sapp, D. J. Fornari, T. Gregg, M. H. Edwards, W. I. Ridley, and J.F. Bender, Geochemistry and morphology of the crestal plateau of the East Pacific Rise ~9°50' N, *Eos Trans. AGU*, 76(46), Fall Meet. Suppl., F694, 1995
- Perfit, M., D. Fornari, I. Ridley, et al., Recent volcanism in the Siqueiros transform fault: picritic basalts and implications for MORB magma genesis, *Earth Planet. Sci. Letts.*, 141, 91-108, 1996
- Perfit, M.R., W.C. Chadwick, Magmatism at mid-ocean ridges: Constraints from volcanological and geochemical investigations, AGU, submitted 1998
- Peterson, D.W., and R.I. Tilling, Transition of basaltic lava from Pahoehoe to AA, Kilauea volcano, Hawaii: Field observations and key factors, *J. Volcanology and Geothermal Res.*, 7, 3-4, 271-293, 1980

- Rowland, S.K., and G.P. Walker, Pahoehoe and aa in Hawaii: Volumetric flow rate controls the lava structure, *Bull. Of Volcanology*, 52, 615-628, 1990
- Rubin, K.H., J.D. Macdougall, and M.R. Perfit,  $^{210}\text{Po}$ - $^{210}\text{Pb}$  dating of recent volcanic eruptions on the sea floor, *Nature*, 368, 841-844, 1994
- Scheirer, D. S., and K. C. Macdonald, Variation in cross-sectional area of the axial ridge along the East Pacific Rise: Evidence for the magmatic budget of a fast spreading center, *J. Geophys. Res.*, 98, 22,321-22,338, 1993
- Shank, T.M., D.J. Fornari, K.L. Von Damm, M.D. Lilley, R.M. Haymon, and R.A. Lutz, Temporal and Spatial Patterns of Biological Community Development at Nascent Deep-Sea Hydrothermal Vents (9°50'N EPR), *Deep Sea Res.*, in press, 1997
- Shaw, H.R., Rheology of basalt in the melting range, *J. of Petrology*, 10, 3, 510-535, 1969
- Sims K., D. Fornari, S. Goldstein, et al., U-series analyses of young lavas from 9-10°N East Pacific Rise: constraints on magma transport and storage times beneath the ridge axis, *Trans. American Geophys. U., EOS*, 78, 792, 1997.
- Sinton, J.M. and R.S. Detrick, 1992, Mid-ocean ridge magma chambers, *J. Geophys. Res.*, 97:197-216.
- Smith, M.C., Perfit, M.R., R. Embley, and W. W. Chadwick, Interpretation of magmatic activity and crustal accretion along the CoAxial and Axial seamount north rift zone: using combined acoustic and geochemical data to map the seafloor at the scale of individual flows, *Trans. Am. Geophys. Union, EOS*, 78, F676, 1997
- Storms, M.A., R. Batiza, Ocean Drilling Program; Leg 142; preliminary report; East Pacific Rise, Engineering Preliminary Report - Ocean Drilling Program, 3, 33 p., 1992.
- Thompson, G., Bryan, W. B., Ballard, R., Hamuro, K., Melson, W. G., Axial processes along a segment of the East Pacific Rise, 10° -12° N, *Nature (London)*, 318 (6045), 429-433
- Walker, G.P.L., Lengths of lava flows, *Royal Soc. of London Philosophical Tran.*, A274, 107-118, 1973
- Wright, D.J., R.M. Haymon, D.J. Fornari, Crustal fissuring and its relationship to magmatic and hydrothermal processes on the East Pacific Rise crest (9°12' to 54' N), *J. Geophys. Res.*, 100:B4, 6097-6120, 1995